QUARTERLY OF APPLIED MATHEMATICS
VOLUME , NUMBER 0
XXXX XXXX, PAGES 000–000
S 0033-569X(XX)0000-0

UNSUPERVISED LEARNING OF COMPOSITIONAL SPARSE CODE FOR NATURAL IMAGE REPRESENTATION

By

YI HONG (*Department of Computer Science, University of California, Los Angeles*),

ZHANGZHANG SI (*Google Inc.*),

WENZE HU (*Department of Statistics, University of California, Los Angeles*),

SONG-CHUN ZHU (*Department of Statistics, University of California, Los Angeles*),

AND

YING NIAN WU (*Department of Statistics, University of California, Los Angeles*)

Abstract.

This article proposes an unsupervised method for learning compositional sparse code for representing natural images. Our method is built upon the original sparse coding framework where there is a dictionary of basis functions often in the form of localized, elongated and oriented wavelets, so that each image can be represented by a linear combination of a small number of basis functions automatically selected from the dictionary. In our compositional sparse code, the representational units are composite: they are compositional patterns formed by the basis functions. These compositional patterns can be viewed as shape templates. We propose an unsupervised learning method for learning a dictionary of frequently occurring templates from training images, so that each training image can be represented by a small number of templates automatically selected from the learned dictionary. The compositional sparse code approximates the raw image of a large number of pixel intensities using a small number of templates, thus facilitating the signal to symbol transition and allowing a symbolic description of the image. The current form of our model consists of two layers of representational units (basis functions and shape templates). It is possible to extend it to multiple layers of hierarchy. Experiments show that our method is capable of learning meaningful compositional sparse code, and the learned templates are useful for image classification.

2000 *Mathematics Subject Classification.* Primary 62M40.

E-mail address: yihong@cs.ucla.edu
E-mail address: zhangzhang.si@gmail.com
E-mail address: wenzehu@ucla.edu
E-mail address: sczhu@stat.ucla.edu
E-mail address: ywu@stat.ucla.edu

1. Introduction.

1.1. *Motivation and objectives.* As illustrated by Figure 1, the ancient Chinese developed the early form of Chinese characters as a coding scheme for representing natural images where each character is a pictorial description of a pattern. The early pictorial form then gradually evolved into the form that is in use today. The system of Chinese characters can be considered a compositional sparse code: each natural image can be described by a small number of characters selected from the dictionary, and each character is a composition of a small number of strokes (the strokes become more pronounced in the more evolved forms of the Chinese characters).

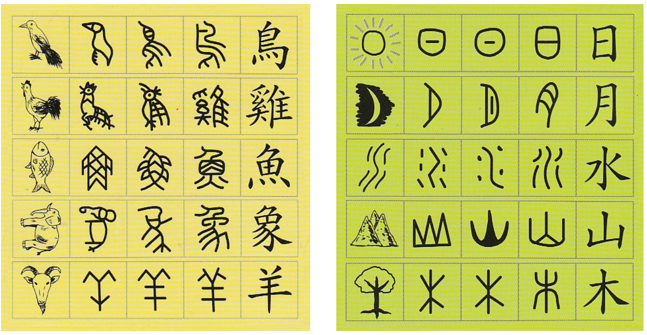

FIG. 1. Chinese characters evolved from representations of natural images of objects and scenes [19]. In each row, the first block shows a picture of the object, and the rest four blocks display the evolution of the corresponding Chinese character over time. Left panel: bird, chicken, fish, elephant and goat. Right panel: sun, moon, water, mountain and wood.

The goal of this paper is to develop a compositional sparse code for natural images. Our coding scheme can be viewed as a mathematical realization of the system of the Chinese characters. In our compositional sparse code, each "stroke" is a linear basis function such as a Gabor wavelet [6] (see Figure 2 for an illustration), and each "character" is a compositional pattern or a shape template formed by a small number of basis functions. We propose an unsupervised learning method for learning frequently occurring templates from training images, so that each training image can be represented by a small number of templates automatically selected from the learned dictionary. Our current compositional sparse code is not a lossless code yet, and it provides approximations to the original images. It translates the original raw image of a large number of pixel intensities into a small number of templates, thus facilitating the signal to symbol transition and allowing a symbolic description of the image. Our experiments show that our method is capable of learning meaningful compositional sparse code. Experiments also show that the learned templates can be useful for image classification. For example, it enables us to learn meaningful "words" in the so-called "bag-of-words" classification scheme.

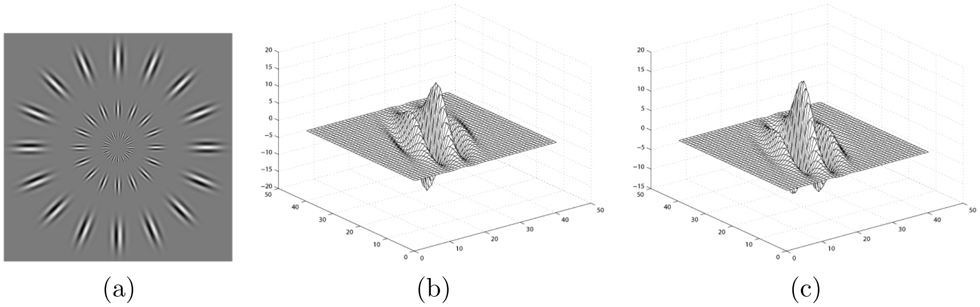

Fig. 2. The Gabor wavelets are Gaussian modulated sine and cosine waves. They serve as basis functions that can be linearly combined to represent natural images. (a) A sample of Gabor wavelets at different locations, orientations and scales. (b) A Gabor sine wavelet. (c) A Gabor cosine wavelet. The Gabor wavelets can be truncated to have finite support (and length).

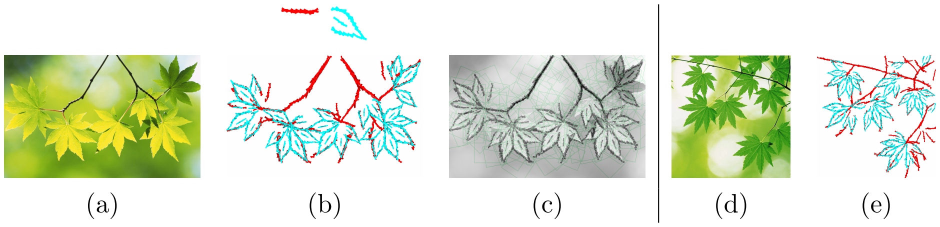

Fig. 3. Unsupervised learning of compositional sparse code (a,b,c) and using it for recognition and segmentation (d,e). (a) Training image of 480 × 768 pixels. (b) Above: 2 compositional patterns (twig and leaf) in the form of shape templates learned from the training image. Size of each template is 100 × 100 pixels. Number of basis functions in each template is no more than 40 and is automatically determined. Below: Representing the training image by translated, rotated, scaled and deformed copies of the 2 templates. (c) Superposing the deformed templates on the original image. Green squared boxes are bounding boxes of the templates. (d) Testing image. (e) Representation (recognition) of the testing image by the 2 templates.

Figure 3 illustrates the basic idea. We start with a dictionary of Gabor wavelets centered at a dense collection of locations and tuned to a collection of scales and orientations. In Figure 3, each Gabor wavelet is illustrated by a bar at the same location and with the same length and orientation as the corresponding wavelet. Figure 3.(a) displays the training image. (b) displays a mini-dictionary of 2 compositional patterns of wavelets learned from the training image. Each compositional pattern is a template formed by a group of a small number of wavelets at selected locations and orientations. The learning is unsupervised in the sense that the images are not labeled or annotated. The number of templates in the dictionary is automatically determined by an adjusted Bayesian information criterion. The 2 templates are displayed in different colors, so that it can be seen clearly how the translated, rotated, scaled and deformed copies of the 2 templates are used to represent the training image, as shown in (b). In (c), the templates are overlaid on the original image, where each green squared box is the bounding box of the template. In our current implementation, we allow some overlap between the bounding boxes of the templates. The templates learned from the training image can be generalized to testing images, as shown in (d) and (e).

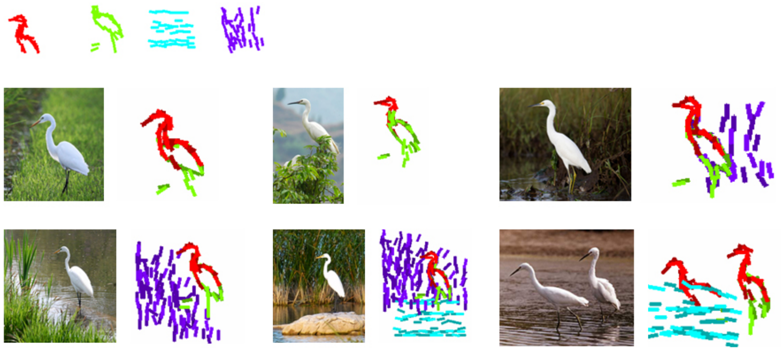

Fig. 4. Another example. Four compositional patterns (templates) are learned unsupervisedly from 20 training images (just 6 of them are shown in figure). The bounding box size for each of the templates is 100 × 100. The numbers of basis functions (Gabor wavelets in our experiments) are less than 40, and the actual numbers are automatically determined.

Figure 4 shows another example, where part templates of egrets and templates of water waves and grasses are learned from 20 training images without supervision. That is, the training images are not registered, in that we do not assume that the objects in the training images appear at the same location and scale. It is interesting to observe that in this example, the unsupervised learning also accomplishes image segmentation, object detection and perceptual grouping (e.g., grass pattern), which are important tasks in vision.

Our compositional sparse code combines two fundamental principles in image representation and computational vision, namely, *sparsity* and *compositionality*. We shall briefly review these two principles below and then give an overview of our methodology.

1.2. *Sparsity and its limitation.* Recent years have seen a flurry of research activities on sparsity in applied mathematics, statistics and machine learning. Sparsity also plays a fundamental role in representing natural images (mathematically, each image can be considered a function defined on a two-dimensional domain, such as a lattice). According to the sparsity principle [26], there is a dictionary of basis functions defined on the same image domain, so that each natural image can be represented by a linear superposition of a small number of basis functions automatically selected from the dictionary. By enforcing sparsity, Olshausen and Field [26] were able to learn a dictionary of basis functions from natural image patches, and these basis functions resemble Gabor wavelets at different locations, orientations and scales. The Gabor wavelets are considered a mathematical model for the so-called simple cells in the primary visual cortex or V1 [6].

Olshausen and Field proposed that the role of V1 is to infer sparse representations of natural images.

The dictionary learned by Olshausen and Field is over-complete, meaning that the number of basis functions in the dictionary is greater than the number of pixels in the image domain. An advantage of such an over-complete dictionary is that the basis functions in this redundant dictionary can afford to be specific enough so that each image can be represented by only a small number of basis functions selected from the dictionary. A popular method for selecting the basis functions from a given dictionary is matching pursuit [22], which is a greedy algorithm that selects one basis function in each iteration, which seeks the maximal reduction in the least squares reconstruction error. A related method is basis pursuit [3] or Lasso [33], which selects the basis functions by solving a penalized least squares problem where the penalty is in the form of the ℓ_1 norm of the coefficients of the basis functions.

In the sparse coding framework, the basis functions in the dictionary exist individually without any structures imposed on them, and the coefficients of these basis functions are usually assumed to be independent of each other. Such simplified independence assumption is clearly inadequate for modeling the wide varieties of patterns in natural images. It is necessary to discover patterns and structures in the selected basis functions.

1.3. *Compositionality and structured sparsity.* The compositionality principle was proposed in the context of computer vision by Geman, Potter, and Chi [15] and Zhu and Mumford [42]. The principle holds that patterns in natural images are compositions of parts, which are themselves compositions of sub-parts, and so on. An interesting example cited by Geman et al. is Laplace's remark that one strongly prefers to view the string CONSTANTINOPLE as a single word, rather than 14 individual letters. This is also the case with the basis functions in the sparse coding of natural images. Like letters forming the words, the basis functions in the sparse representations of natural images also form various compositional patterns in terms of their spatial arrangements. We call such sparsity the compositional sparsity, which is a special form of structured sparsity.

Structured sparsity has received considerable attention in statistics and machine learning in recent years. The most prominent example is the group Lasso [38], which replaces the ℓ_1 penalty of Lasso by a composite penalty based on the group structure among the basis functions. In the group Lasso, the collection of the groups is assumed given. In our work, however, we do not assume that the groups are given, and we seek to learn dictionaries of the recurring compositional patterns in the spatial grouping of the basis functions.

Any hierarchical compositional model will necessarily end with constituent elements that cannot be further decomposed, and such elements may be called "atoms." Interestingly, the basis functions are commonly referred to as atoms in sparse coding literature, and the sparse representation based on atoms is usually called "atomic decomposition" [22, 8]. Compositionality enables us to compose atoms into composite representational units, which leads to much sparser and thus more meaningful representations of the signals.

The current form of our model consists of two layers of representational units (basis functions and shape templates). It is possible to extend it to multiple layers of hierarchy.

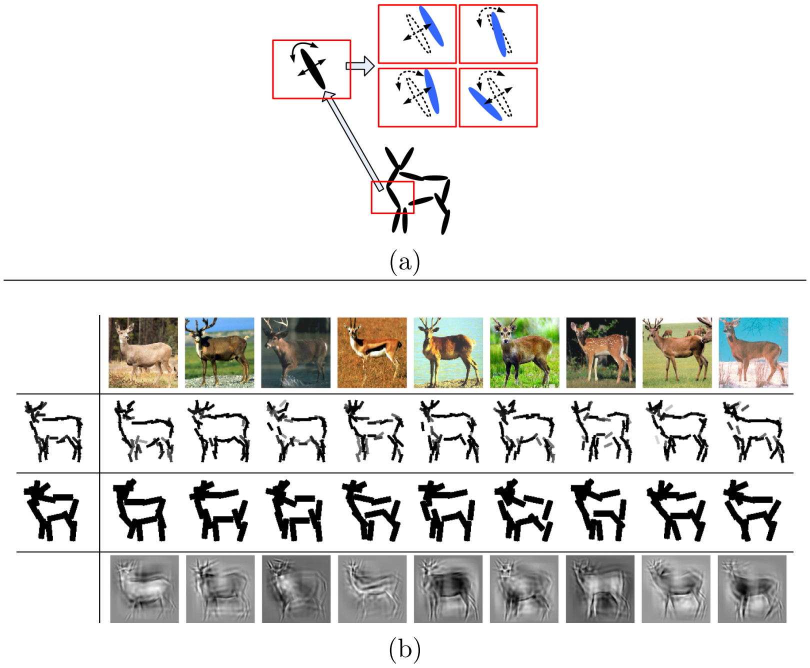

Fig. 5. (a) An active basis model is a composition of a small number of basis functions, each is a Gabor wavelet and is illustrated by a bar with the same location, orientation and length. Each basis function can perturb its location and orientation. (b) Supervised learning of active basis model from aligned images. In this example, two active basis models are learned using Gabor wavelets at two different scales (there is no variation in the aspect ratio of the Gabor wavelets used). The first row displays the 9 training images. The second row: the first plot is the nominal template formed by 50 basis functions. The rest of the plots are the deformed templates matched to the images. The third row: the same as the second row, except that the scale of the Gabor wavelets is about twice as large, and the number of wavelets is 14. The last row displays the linear reconstruction of each training image from 100 selected and perturbed basis functions.

1.4. *Overview of our methodology.* In this article, we assume that the dictionary of basis functions is given, and they are Gabor wavelets at a dense collection of locations, orientations and scales. We focus on learning compositional patterns formed by these basis functions. In principle, the basis functions can also be learned from training images.

We represent each compositional pattern of basis functions by an active basis model of Wu et al. [37], which is a composition of a small number of basis functions automatically selected from a given dictionary. The selected basis functions are allowed to perturb their locations and orientations so that the linear basis formed by the selected basis functions become active and the active basis can be viewed a deformable template. Figure 5 illustrates the basic idea of the active basis model.

Wu et al. mainly studied the problem of learning a single active basis model from a set of aligned training images, where the images are defined on the same bounding box, and the objects in the images are from the same category, in the same pose, and appear at the same location and scale. The learning of the active basis model in this situation can be called supervised learning.

Our work goes far beyond Wu et al. In our work, the training images are not assumed to be aligned, and each image can be represented by multiple active basis templates. That is, the active basis models serve as the composite representational units in our compositional sparse code. For a given set of training images, our method is to learn a dictionary of active basis templates, so that each training image can be represented by a small number of templates that are translated, rotated, scaled and deformed copies of the learned templates in the dictionary.

The unsupervised learning algorithm is initialized from random templates. The algorithm then iterates the following two steps:

(1) Image encoding: Encode each training image by translated, rotated, scaled and deformed copies of the templates in the current dictionary, by a template matching pursuit process.

(2) Dictionary learning: Re-learn each template from image patches currently encoded by this template, by a shared matching pursuit process.

The rest of the paper is organized as follows. Section 2 reviews the original sparse coding framework and the active basis model. Section 3 presents our representational scheme and the unsupervised learning algorithm. Section 4 describes experimental results on image representation and classification. Section 5 concludes with a discussion.

2. Background: sparse coding model and active basis model.

This section reviews sparse coding model and the active basis model in order to fix the notation and set the stage for presenting our model and learning algorithm in the next section.

2.1. *Olshausen-Field model for sparse coding.* Olshausen and Field [26] proposed that the role of simple V1 cells is to compute sparse representations of natural images. Let $\{\mathbf{I}_m, m = 1, ..., M\}$ be a set of small image patches. For example, they might be 12×12 patches, in which case $\mathbf{I}_m \in \mathrm{R}^{12\times 12}$. We may think of each $\mathbf{I}_m$ as a two-dimensional function defined on the 12×12 lattice. The Olshausen-Field model seeks to represent these images by

$$\mathbf{I}_m = \sum_{i=1}^{N} c_{m,i} B_i + U_m, \tag{2.1}$$

where $(B_i, i = 1, ..., N)$ is a dictionary of basis functions defined on the same image lattice (e.g., 12×12) as $\mathbf{I}_m$, $c_{m,i}$ are the coefficients, and U_m is the unexplained residual image. N is often assumed to be greater than the number of pixels in $\mathbf{I}_m$, so the dictionary is said to be over-complete and is therefore redundant. However, the number of coefficients $(c_{m,i}, i = 1, ..., N)$ that are non-zero (or significantly different from zero) is assumed to be small (e.g., less than 10) for each image $\mathbf{I}_m$.

Geometric attributes. One may also assume that the basis functions in the dictionary are translated, rotated and dilated versions of one another, as in [27], so that each B_i can be written as $B_{x,s,\alpha}$, where x is the location (a two-dimensional vector), s is the scale, and α is the orientation. We call such a dictionary self-similar, and we call (x, s, α) the geometric attribute of $B_{x,s,\alpha}$.

Model (2.1) then becomes

$$\mathbf{I}_m = \sum_{x,s,\alpha} c_{m,x,s,\alpha} B_{x,s,\alpha} + U_m, \tag{2.2}$$

where $B_{x,s,\alpha}$ are translated, rotated and dilated copies of a single basis function, e.g., $B = B_{x=0,s=1,\alpha=0}$, and (x, s, α) are properly discretized (default setting: α is discretized into 16 equally spaced orientations). B can be learned from training images $\{\mathbf{I}_m\}$ [27].

Assumption on basis functions in this paper. From now on, we assume that the dictionary of basis functions is self-similar, and $\{B_{x,s,\alpha}, \forall(x, s, \alpha)\}$ is already given. In the following, we assume that $B_{x,s,\alpha}$ is a Gabor wavelet, and we also assume that $B_{x,s,\alpha}$ is normalized to have unit ℓ_2 norm so that $|B_{x,y,\alpha}|^2 = 1$. $B_{x,s,\alpha}$ may also be a pair of Gabor sine and cosine wavelets, so that for each Gabor wavelet B, $B = (B_0, B_1)$. The corresponding coefficient $c = (c_0, c_1)$, and $cB = c_0B_0 + c_1B_1$. The projection $\langle \mathbf{I}, B\rangle = (\langle \mathbf{I}, B_0\rangle, \langle \mathbf{I}, B_1\rangle)$, and $|\langle \mathbf{I}, B\rangle|^2 = \langle \mathbf{I}, B_0\rangle^2 + \langle \mathbf{I}, B_1\rangle^2$.

Spatial point process. Given the dictionary $(B_{x,s,\alpha}, \forall(x, s, \alpha))$, the encoding of an image $\mathbf{I}_m$ amounts to inferring $(c_{m,x,s,\alpha}, \forall(x, s, \alpha))$ in (2.2) under the sparsity constraint, which means that only a small number of $(c_{m,x,s,\alpha})$ are non-zero. That is, we seek to encode $\mathbf{I}_m$ by

$$\mathbf{I}_m = \sum_{i=1}^{n} c_{m,i} B_{x_{m,i},s_{m,i},\alpha_{m,i}} + U_m, \tag{2.3}$$

where $n \ll N$ is a small number, and $(x_{m,i}, s_{m,i}, \alpha_{m,i}, i = 1, ..., n)$ are the geometric attributes of the selected basis functions whose coefficients $(c_{m,i})$ are non-zero. The attributes $(x_{m,i}, s_{m,i}, \alpha_{m,i}, i = 1, ..., n)$ form a spatial point process (we continue to use i to index the basis functions, but here i only runs through the n selected basis functions instead of all the N basis functions as in (2.1)).

2.2. *Active basis model for shared sparse coding of aligned image patches.* The active basis model was proposed by Wu et al. [37] for modeling deformable templates formed by basis functions.

Suppose we have a set of training image patches $\{\mathbf{I}_m, m = 1, ..., M\}$. This time we assume that they are defined on the same bounding box, and the objects in these images come from the same category. In addition, these objects appear at the same location, scale and orientation, and in the same pose. See Figure 5 for 9 image patches of deer. We call such image patches aligned.

The active basis model is of the following form

$$\mathbf{I}_m = \sum_{i=1}^{n} c_{m,i} B_{x_i+\Delta x_{m,i},s,\alpha_i+\Delta\alpha_{m,i}} + U_m, \tag{2.4}$$

where $\mathbf{B} = (B_{x_i,s,\alpha_i}, i = 1, ..., n)$ form the nominal template of an active basis model (sometimes we simply call $\mathbf{B}$ an active basis template). Here we assume that the scale s is fixed and given. $\mathbf{B}_m = (B_{x_i+\Delta x_{m,i},s,\alpha_i+\Delta\alpha_{m,i}}, i = 1, ..., n)$ is the deformed version of the nominal template $\mathbf{B}$ for encoding $\mathbf{I}_m$, where $(\Delta x_{m,i}, \Delta\alpha_{m,i})$ are the perturbations of the location and orientation from the nominal location x_i and the nominal orientation α_i

respectively. The perturbations are introduced to account for shape deformation. Both $\Delta x_{m,i}$ and $\Delta \alpha_{m,i}$ are assumed to vary within limited ranges (default setting: $\Delta x_{m,i} \in [-3, 3]$ pixels, and $\Delta \alpha_{m,i} \in \{-1, 0, 1\} \times \pi/16$).

2.3. *Prototype algorithm.* Given the dictionary of basis functions $\{B_{x,s,\alpha}, \forall x, s, \alpha\}$, the learning of the active basis model from the aligned image patches $\{\mathbf{I}_m\}$ involves the sequential selection of B_{x_i,s,α_i} and the inference of its perturbed version $B_{x_i+\Delta x_{m,i},s,\alpha_i+\Delta\alpha_{m,i}}$ in each image $\mathbf{I}_m$. We call the learning as supervised, because the bounding boxes of the objects are given and the images are aligned. See Figure 5 for an illustration of the learning results.

In this subsection, we consider a prototype version of the shared matching pursuit algorithm, which is to be revised in the following subsections. The reason we start from this prototype algorithm is that it is simple and yet captures the key features of the learning algorithm.

The prototype algorithm is a greedy algorithm that seeks the maximal reduction of the following least squares reconstruction error in each iteration (recall that the basis functions are normalized to have unit ℓ_2 norm):

$$\sum_{m=1}^{M} |\mathbf{I}_m - \sum_{i=1}^{n} c_{m,i} B_{x_i+\Delta x_{m,i},s,\alpha_i+\Delta\alpha_{m,i}}|^2. \tag{2.5}$$

[0] Initialize $i \leftarrow 0$. For $m = 1, ..., M$, initialize the residual image $U_m \leftarrow \mathbf{I}_m$.

[1] $i \leftarrow i + 1$. Select the next basis function by

$$(x_i, \alpha_i) = \arg\max_{x,\alpha} \sum_{m=1}^{M} \max_{\Delta x, \Delta\alpha} |\langle U_m, B_{x+\Delta x,s,\alpha+\Delta\alpha}\rangle|^2,$$

where $\max_{\Delta x,\Delta\alpha}$ is local maximum pooling within the small ranges of $\Delta x_{m,i}$ and $\Delta\alpha_{m,i}$.

[2] For $m = 1, ..., M$, given (x_i, α_i), infer the perturbations in location and orientation by retrieving the arg-max in the local maximum pooling of step [1]:

$$(\Delta x_{m,i}, \Delta\alpha_{m,i}) = \arg\max_{\Delta x,\Delta\alpha} |\langle U_m, B_{x_i+\Delta x,s,\alpha_i+\Delta\alpha}\rangle|^2. \tag{2.6}$$

Let $c_{m,i} \leftarrow \langle U_m, B_{x_i+\Delta x_{m,i},s,\alpha_i+\Delta\alpha_{m,i}}\rangle$, and update the residual image by explaining away:

$$U_m \leftarrow U_m - c_{m,i} B_{x_i+\Delta x_{m,i},s,\alpha_i+\Delta\alpha_{m,i}}. \tag{2.7}$$

[3] Stop if $i = n$, else go back to step [1].

Simultaneous (or collaborative) sparse approximation of multiple signals has been proposed in harmonic analysis and signal processing literature [4, 32]. However, perturbations of selected basis functions are not considered in [4, 32].

Assumption on orthogonality in this paper. In Equation (2.7), the perturbed basis function $B_{x_i+\Delta x_{m,i},s,\alpha_i+\Delta\alpha_{m,i}}$ explains away part of U_m. As a result, nearby basis functions that overlap with $B_{x_i+\Delta x_{m,i},s,\alpha_i+\Delta\alpha_{m,i}}$ tend not to be selected in future iterations. So the basis functions selected for each deformed template $\mathbf{B}_m = (B_{x_i+\Delta x_{m,i},s,\alpha_i+\Delta\alpha_{m,i}}, i = 1, \cdots, n)$ usually have little overlap with each other. For computational and modeling convenience, we shall assume that these selected basis functions are orthogonal to each other, so that the coefficients can be obtained by projection: $c_{m,i} = \langle \mathbf{I}_m, B_{x_i+\Delta x_{m,i},s,\alpha_i+\Delta\alpha_{m,i}}\rangle$.

Correspondingly, the explaining-away step can then be carried out by local inhibition. Specifically, after we identify the perturbed basis function $B_{x_i+\Delta x_{m,i},s,\alpha_i+\Delta\alpha_{m,i}}$, we simply prohibit nearby basis functions that are correlated with $B_{x_i+\Delta x_{m,i},s,\alpha_i+\Delta\alpha_{m,i}}$ from being included in the deformed template $\mathbf{B}_m$. In practice, we allow small correlations between the basis functions in each $\mathbf{B}_m$.

2.4. *Statistical modeling.* The above algorithm guided by (2.5) implicitly assumes that the unexplained background image U_m is Gaussian white noise. This assumption can be problematic because the unexplained background may contain salient structures such as edges, and the Gaussian white noise distribution clearly cannot account for such structures. This is why we need to revise the above algorithm which is based on the Gaussian white noise assumption. A better assumption is to assume that U_m follows the same distribution as that of natural images.

Density substitution. More precisely, the distribution of $\mathbf{I}_m$ given the deformed template $\mathbf{B}_m = (B_{x_i+\Delta x_{m,i},s,\alpha_i+\Delta\alpha_{m,i}}, i = 1, ..., n)$, i.e., $p(\mathbf{I}_m \mid \mathbf{B}_m)$, is obtained by modifying the distribution of natural images $q(\mathbf{I}_m)$ in such a way that we only change the distribution of $C_m = (c_{m,i} = \langle \mathbf{I}_m, B_{x_i+\Delta x_{m,i},s,\alpha_i+\Delta\alpha_{m,i}}\rangle, i = 1, ..., n)$ from $q(C_m)$ to $p(C_m)$, while leaving the conditional distribution of U_m given C_m unchanged. Here $p(C_m)$ and $q(C_m)$ are the distributions of C_m under $p(\mathbf{I}_m \mid \mathbf{B}_m)$ and $q(\mathbf{I}_m)$ respectively. Thus the model is in the form of foreground $p(C_m)$ popping out from background $q(\mathbf{I}_m)$. Specifically, $p(\mathbf{I}_m \mid \mathbf{B}_m) = q(\mathbf{I}_m)p(C_m)/q(C_m)$.

Such a density substitution scheme was first used in projection pursuit density estimation [14], see also [16]. The reason for such a form is as follows. C_m is the projection of $\mathbf{I}_m$ into $\mathbf{B}_m$. Let U_m be the projection of $\mathbf{I}_m$ into the remaining subspace that is orthogonal to $\mathbf{B}_m$. Then $p(\mathbf{I}_m \mid \mathbf{B}_m)/q(\mathbf{I}_m) = p(C_m, U_m)/q(C_m, U_m) = p(C_m)/q(C_m)$. The second equality follows from the assumption that $p(U_m|C_m) = q(U_m|C_m)$, i.e., we keep the conditional distribution of U_m given C_m fixed.

For computational simplicity, we further assume $(c_{m,i} = \langle \mathbf{I}_m, B_{x_i+\Delta x_{m,i},s,\alpha_i+\Delta\alpha_{m,i}}\rangle, i = 1, ..., n)$ are independent given $\mathbf{B}_m$, under both p and q, so

$$p(\mathbf{I}_m \mid \mathbf{B}_m) = q(\mathbf{I}_m)\prod_{i=1}^{n}\frac{p_i(c_{m,i})}{q(c_{m,i})},$$

where $q(c)$ is assumed to be the same for $i = 1, ..., n$ because $q(\mathbf{I}_m)$ is translation and rotation invariant. $q(c)$ can be pooled from natural images in the form of a histogram of Gabor filter responses. This histogram is heavy-tailed because of the edges in natural images.

Exponential family model. For parametric modeling, we model $p_i(c_{m,i})/q(c_{m,i})$ in the form of exponential family model. Specifically, we assume the following exponential family model $p_i(c) = p(c; \lambda_i)$, which is in the form of exponential tilting of the reference distribution $q(c)$:

$$p(c; \lambda) = \frac{1}{Z(\lambda)}\exp\{\lambda h(|c|^2)\}q(c), \tag{2.8}$$

so that $p(c; \lambda)/q(c)$ is in the exponential form. We assume $\lambda_i > 0$. $h(r)$ is a sigmoid-like function of the response $r = |c|^2$ that saturates for large r (recall that the Gabor filter response $c = (c_0, c_1)$ consists of responses from the pair of Gabor sine and cosine wavelets, and $|c|^2 = c_0^2 + c_1^2)$. Specifically, we assume that $h(r) = \xi[2/(1+e^{-2r/\xi}) - 1]$, so $h(r) \approx r$ for small r, and $h(r) \to \xi$ as $r \to \infty$ (default setting: $\xi = 6$). The reason we want $h(r)$ to approach a fixed constant for large r is that there can be strong edges in both the foreground and background, albeit with different frequencies. $p(c;\lambda)/q(c)$ should approach the ratio between these two frequencies for large $r = |c|^2$. In (2.8),

$$Z(\lambda) = \int \exp\{\lambda h(r)\} q(c) dc = \mathrm{E}_q[\exp\{\lambda h(r)\}]$$

is the normalizing constant.

$$\mu(\lambda) = \mathrm{E}_\lambda[h(r)] = \int h(r) p(c;\lambda) dc$$

is the mean parameter. Both $Z(\lambda)$ and $\mu(\lambda)$ can be computed beforehand from a set of natural images.

Information theoretical interpretation. The exponential family model can be justified by the maximum entropy principle [28, 43, 16, 36]. Given the deformed template $\mathbf{B}_m = (B_{x_i+\Delta x_{m,i}, s, \alpha_i + \Delta\alpha_{m,i}}, i = 1, ..., n)$, consider the coefficients obtained by projection: $(c_{m,i}(\mathbf{I}_m) = \langle \mathbf{I}_m, B_{x_i+\Delta x_{m,i}, s, \alpha_i+\Delta\alpha_{m,i}} \rangle, i = 1, ..., n)$. Suppose we want to find a probability distribution $p(\mathbf{I}_m \mid \mathbf{B}_m)$ so that $\mathrm{E}[h(|c_{m,i}(\mathbf{I}_m)|^2)] = \mu_i$ for some fixed μ_i, $i = 1, ..., n$, where μ_i can be estimated from the training images. Then among all the distributions that satisfy the constraints on $\mathrm{E}[h(|c_{m,i}(\mathbf{I}_m)|^2)]$, the distribution that is closest to $q(\mathbf{I}_m)$ in terms of the Kullback-Leibler divergence is given by

$$p(\mathbf{I}_m \mid \mathbf{B}_m) = \frac{1}{Z(\Lambda)} \exp\{\sum_{i=1}^n \lambda_i h(|c_{m,i}(\mathbf{I}_m)|^2)\} q(\mathbf{I}_m),$$

where $\Lambda = (\lambda_i, i = 1, ..., n)$, $Z(\Lambda) = \mathrm{E}_q[\exp\{\sum_{i=1}^n \lambda_i h(|c_{m,i}(\mathbf{I}_m)|^2)]$ is the normalizing constant, and Λ is chosen to satisfy the constraints on $\mathrm{E}[h(|c_{m,i}(\mathbf{I}_m)|^2)]$. If we further assume that $c_{m,i}(\mathbf{I}_m)$ are independent of each other for $i = 1, ..., n$ under $q(\mathbf{I}_m)$, then $c_{m,i}(\mathbf{I}_m)$ are also independent under $p(\mathbf{I}_m \mid \mathbf{B}_m)$, and their distributions are of the form (2.8).

In order to choose the nominal template $\mathbf{B}$ and the deformed templates $\{\mathbf{B}_m, m = 1, ..., M\}$, we want $p(\mathbf{I}_m \mid \mathbf{B}_m)$ to be farthest from $q(\mathbf{I}_m)$ in terms of Kullback-Leibler divergence. From a classification point of view, we want to choose $\mathbf{B}$ and $\{\mathbf{B}_m\}$ so that the features $\{h(|c_{m,i}|^2), i = 1, ..., n\}$ lead to the maximal separation between training images (e.g., images of deer) and generic natural images.

Log-likelihood ratio. The log-likelihood ratio between the current model $p(\mathbf{I}_m|\mathbf{B}_m)$ and the reference model $q(\mathbf{I}_m)$ is

$$l(\{\mathbf{I}_m\} \mid \mathbf{B}, \{\mathbf{B}_m\}, \Lambda) = \sum_{m=1}^M \log \frac{p(\mathbf{I}_m|\mathbf{B}_m)}{q(\mathbf{I}_m)} \tag{2.9}$$

$$= \sum_{m=1}^M \sum_{i=1}^n \left[\lambda_i h(|\langle \mathbf{I}_m, B_{x_i+\Delta x_{m,i}, s, \alpha_i+\Delta\alpha_{m,i}} \rangle|^2) - \log Z(\lambda_i)\right]. \tag{2.10}$$

The expectation of the above log-likelihood ratio is the Kullback-Leibler divergence between $p(\mathbf{I}_m \mid \mathbf{B}_m)$ and $q(\mathbf{I}_m)$.

Given the training images $\{\mathbf{I}_m, m = 1, ..., M\}$, $\sum_{m=1}^{M} \log q(\mathbf{I}_m)$ is a constant. Thus maximizing the log-likelihood ratio $\sum_{m=1}^{M} \log p(\mathbf{I}_m \mid \mathbf{B}_m, \Lambda)/q(\mathbf{I}_m)$ is equivalent to maximizing the log-likelihood $\sum_{i=1}^{M} \log p(\mathbf{I}_m \mid \mathbf{B}_m, \Lambda)$. So in the following, with a slight abuse of terminology, we occasionally refer to the log-likelihood ratio as the log-likelihood.

2.5. *Shared matching pursuit.* We revise the prototype algorithm in subsection (2.3) so that each iteration seeks the maximal increase of the log-likelihood ratio (2.10) instead of the maximum reduction of the least squares reconstruction error (2.5) as in subsection (2.3). The revised version of the shared matching pursuit algorithm is as follows.

[0] Initialize $i \leftarrow 0$. For $m = 1, ..., M$, initialize the response maps $R_m(x, \alpha) \leftarrow \langle \mathbf{I}_m, B_{x,s,\alpha} \rangle$ for all (x, α).

[1] $i \leftarrow i + 1$. Select the next basis function by finding

$$(x_i, \alpha_i) = \arg\max_{x,\alpha} \sum_{m=1}^{M} \max_{\Delta x, \Delta\alpha} h(|R_m(x + \Delta x, \alpha + \Delta\alpha)|^2),$$

where $\max_{\Delta x, \Delta\alpha}$ is again local maximum pooling.

[2] For $m = 1, ..., M$, given (x_i, α_i), infer the perturbations by retrieving the arg-max in the local maximum pooling of step [1]:

$$(\Delta x_{m,i}, \Delta\alpha_{m,i}) = \arg\max_{\Delta x, \Delta\alpha} |R_m(x_i + \Delta x, \alpha_i + \Delta\alpha)|^2.$$

Let $c_{m,i} \leftarrow R_m(x_i + \Delta x_{m,i}, \alpha_i + \Delta\alpha_{m,i})$, and update $R_m(x, \alpha) \leftarrow 0$ if the correlation $\text{corr}[B_{x,s,\alpha}, B_{x_i+\Delta x_{m,i},s,\alpha_i+\Delta\alpha_{m,i}}] > \epsilon$ (default setting: $\epsilon = .1$). Then compute λ_i by solving the maximum likelihood equation $\mu(\lambda_i) = \sum_{m=1}^{M} h(|c_{m,i}|^2)/M$.

[3] Stop if $i = n$, else go back to step [1].

Esimtation of λ_i. For each candidate (x_i, α_i), the maximum likelihood equation $\mu(\lambda_i) = \sum_{m=1}^{M} h(|c_{m,i}|^2)/M$ is obtained by taking the derivative of the log-likelihood ratio, where $\mu(\lambda_i) = \text{E}_{\lambda_i}[h(|c|^2)] = \int h(|c|^2) p(c; \lambda_i) dc$ is the mean parameter, and is a monotone increasing function of $\lambda_i > 0$. So its inverse $\mu^{-1}()$ is also a monotone increasing function. λ_i is solved so that $\mu(\lambda_i)$ matches the empirical average of $h(|c_{m,i}|^2)$, $m = 1, ..., M$. The function $\mu()$ can be computed and stored over a discrete set of equal-spaced values, so that λ_i can be solved by looking up these values with linear interpolations between them.

Selection of (x_i, α_i). Because $h()$ is monotonically increasing, the maximized log-likelihood ratio is monotone in the estimated λ_i. The estimated λ_i is in turn monotone in the $\sum_{m=1}^{M} h(|c_{m,i}|^2)/M$. So the maximized log-likelihood ratio is monotone in $\sum_{m=1}^{M} h(|c_{m,i}|^2)/M$. Therefore, in step [1], (x_i, α_i) is chosen by maximizing the sum $\sum_{m=1}^{M} \max_{\Delta x, \Delta\alpha} h(|R_m(x + \Delta x, \alpha + \Delta\alpha)|^2)$ over all possible (x, α).

Arg-max inhibition. In step [2], the arg-max basis function inhibits nearby basis functions to enforce the approximate orthogonality constraint. The correlation is defined as the square of the inner product between the basis functions and can be computed and stored beforehand.

Inference. After learning the template from training images $\{\mathbf{I}_m\}$, we can use the learned template to detect the object in a testing image $\mathbf{I}$.

[1] For every pixel X, compute the log-likelihood ratio $l(X)$, which serves as the template matching score at putative location X:

$$l(X) = \sum_{i=1}^{n} \left[\lambda_i \max_{\Delta x, \Delta\alpha} h(|\langle \mathbf{I}, B_{X+x_i+\Delta x, s, \alpha_i+\Delta\alpha}\rangle|^2) - \log Z(\lambda_i)\right]. \tag{2.11}$$

[2] Find maximum likelihood location $\hat{X} = \arg\max_X l(X)$. For $i = 1, ..., n$, inferring perturbations by retrieving the arg-max in the local maximum pooling in step [1]:

$$(\Delta x_i, \Delta\alpha_i) = \arg \max_{\Delta x, \Delta\alpha} |\langle \mathbf{I}, B_{\hat{X}+x_i+\Delta x, s, \alpha_i+\Delta\alpha}\rangle|^2.$$

[3] Return the location $\hat{X}$, and $(B_{\hat{X}+x_i+\Delta x_i, s, \alpha_i+\Delta\alpha_i}, i = 1, ..., n)$, which is the translated and deformed template.

Rotation and multi-resolution. We can rotate the template and scan the template over multiple resolutions of the original image, to account for uncertainties about the orientation and scale of the object in the testing image.

3. Compositional sparse code: model and algorithm.

In the linear additive sparse coding model $\mathbf{I}_m = \sum_{i=1}^{N} c_{m,i} B_i + U_m$, the coefficients of the basis functions in the dictionary are assumed to be independent. A natural question is how to correct this assumption. Since we argue that the Olshausen-Field model with a dictionary of self-similar basis functions is essentially a spatial point process, we may search for compositional patterns in the spatial arrangements of the basis functions with non-zero coefficients.

In this section, we shall specify our compositional sparse coding model where each representational unit is an active basis model. Then we shall describe the algorithm for learning dictionaries of active basis models from training images.

3.1. *Compositional sparse coding model.* We strive to write down our model in an analogous form as the Olshausen-Field model $\mathbf{I}_m = \sum_{i=1}^{n} c_{m,i} B_{x_{m,i}, s_{m,i}, \alpha_{m,i}} + U_m$, by making the notation compact.

Compact notation. As the first step, let us slightly generalize the active basis model by assuming that the template may appear at location X_m in image $\mathbf{I}_m$, then we can write the representation in the following form:

$$\begin{aligned} \mathbf{I}_m &= \sum_{i=1}^{n} c_{m,i} B_{X_m+x_i+\Delta x_{m,i}, s, \alpha_i+\Delta\alpha_{m,i}} + U_m \\ &= C_m \mathbf{B}_{X_m} + U_m, \end{aligned} \tag{3.1}$$

where $\mathbf{B}_{X_m} = (B_{X_m+x_i+\Delta x_{m,i}, s, \alpha_i+\Delta\alpha_{m,i}}, i = 1, ..., n)$ is the deformed template spatially translated to X_m, $C_m = (c_{m,i}, i = 1, ..., n)$, and $C_m B_{X_m} = \sum_{i=1}^{n} c_{m,i} B_{X_m+x_i+\Delta x_{m,i}, s, \alpha_i+\Delta\alpha_{m,i}}$ by definition.

$\mathbf{B}_{X_m}$ explains the part of $\mathbf{I}_m$ that is covered by $\mathbf{B}_{X_m}$. For each image $\mathbf{I}_m$ and each X_m, we can define the log-likelihood ratio similar to (2.11):

$$\begin{aligned} l(\mathbf{I}_m \mid \mathbf{B}_{X_m}) &= \log \frac{p(\mathbf{I}_m \mid \mathbf{B}_{X_m})}{q(\mathbf{I}_m)} \\ &= \sum_{i=1}^{n} \left[\lambda_i \max_{\Delta x, \Delta \alpha} h(|\langle \mathbf{I}_m, B_{X_m + x_i + \Delta x, s, \alpha_i + \Delta \alpha} \rangle|^2) - \log Z(\lambda_i) \right]. \quad (3.2) \end{aligned}$$

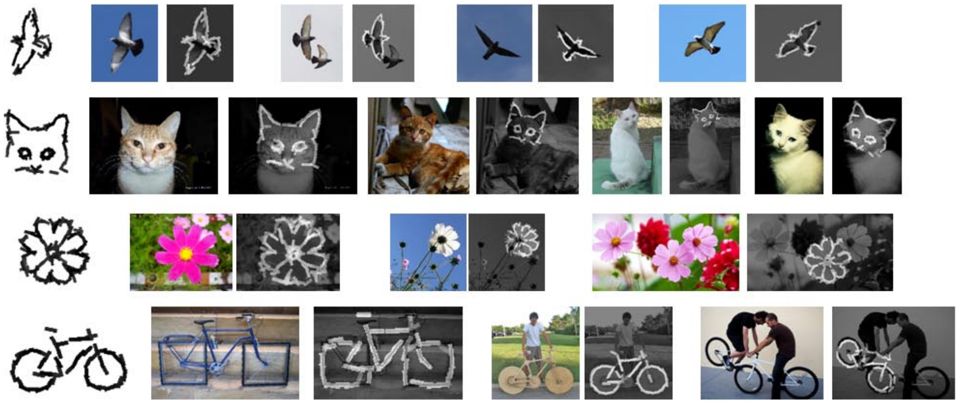

FIG. 6. Objects appear at different locations, scales and orientations in the training images. In each row, the first plot displays the nominal active basis template. The rest of the row displays some examples of training images and the suppositions of the spatially translated, scaled, rotated and deformed versions of the nominal template.

As the next step of this modeling procedure, in addition to spatial translation and deformation, we can also rotate and scale the template. So a more general version of (3.1) is

$$\mathbf{I}_m = C_m \mathbf{B}_{X_m, S_m, A_m} + U_m, \quad (3.3)$$

where X_m is the location, S_m is the scale, and A_m is the orientation of the translated, rotated, scaled and deformed template. The scaling of the template is implemented by changing the resolution of the original image. We adopt the convention that whenever the notation $\mathbf{B}$ appears in image representation, it always means the deformed template, where the perturbations of the basis functions can be inferred by local max pooling. The log-likelihood ratio $l(\mathbf{I}_m \mid \mathbf{B}_{X_m, S_m, A_m})$ can be similarly defined as in (3.2). Figure 6 illustrates the basic idea of representation (3.3). In addition to spatial translation, dilation and rotation of the template, we may also allow mirror reflection as well as the change of aspect ratio.

Compact representation. Now suppose we have a dictionary of T active basis templates, $\{\mathbf{B}^{(t)}, t = 1, ..., T\}$, where each $\mathbf{B}^{(t)}$ is a compositional pattern of basis functions. Then we can represent the image $\mathbf{I}_m$ by K_m templates that are spatially translated, rotated, scaled and deformed versions of these T templates in the dictionary:

$$\mathbf{I}_m = \sum_{k=1}^{K_m} C_{m,k} \mathbf{B}^{(t_{m,k})}_{X_{m,k}, S_{m,k}, A_{m,k}} + U_m, \tag{3.4}$$

where each $\mathbf{B}^{(t_k)}_{X_{m,k}, S_{m,k}, A_{m,k}}$ is obtained by translating the template of type t_k, i.e., $\mathbf{B}^{(t_k)}$, to location $X_{m,k}$, scale it to scale $S_{m,k}$, rotate it to orientation $A_{m,k}$, and deform it to match $\mathbf{I}_m$. Note that according to (3.4), the images represented by the dictionary are no longer assumed to be aligned.

If the K_m templates do not overlap with each other, then the log-likelihood ratio is

$$\sum_{m=1}^{M} \sum_{k=1}^{K_m} \left[l(\mathbf{I}_m \mid \mathbf{B}^{(t_{m,k})}_{X_{m,k}, S_{m,k}, A_{m,k}}) \right]. \tag{3.5}$$

Packing and unpacking. The above representation is in analogy to model (2.3) in subsection (2.1), which we copy here: $\mathbf{I}_m = \sum_{i=1}^{n} c_{m,i} B_{x_{m,i}, s_{m,i}, \alpha_{m,i}} + U_m$. The difference is that each $\mathbf{B}^{(t_k)}_{X_{m,k}, S_{m,k}, A_{m,k}}$ is a composite representational unit, which is itself a group of basis functions that follow a certain compositional pattern of type t_k. Because of such grouping or packing, the number of templates K_m needed to encode $\mathbf{I}_m$ is expected to be much smaller than the total number of basis functions needed to represent $\mathbf{I}_m$, thus resulting in sparser representation. Specifically, if each template is a group of g basis functions, then the number of basis functions in the representation (3.4) is $K_m g$. In fact, we can unpack model (3.4) into the representation (2.3). The reason that it is advantageous to pack the basis functions into groups is that these groups exhibit T types of frequently occurring spatial grouping patterns, so that when we encode the image $\mathbf{I}_m$, for each selected group $\mathbf{B}^{(t_{m,k})}_{X_{m,k}, S_{m,k}, A_{m,k}}$, we only need to code the overall location, scale, orientation and type of the group, instead of the locations, scales and orientations of the individual constituent basis functions.

Limited overlap assumption. It is desirable to allow some limited overlap between the bounding boxes of the K_m templates that encode $\mathbf{I}_m$. Even if the bounding boxes of two templates have some overlap with each other, their constituent basis functions may not overlap much. If we do not allow any overlap between the bounding boxes of the templates, some salient structures of $\mathbf{I}_m$ may fall through the cracks between the templates. Also, it is possible that the frequently occurring patterns may actually overlap with each other. For instance, in a string "ABABABA", the pattern "AB" is frequently occurring, but at the same time, the pattern "BA" is as frequent as "AB", and these two patterns overlap with each other. So it can be desirable to allow some overlap between the patterns in order to recover all the important recurring patterns. On the other hand, we do not want to allow excessive overlap between the templates. Otherwise the learned templates will be too redundant, and we will need a lot of them in order to describe the training images. In practice, we assume the following limited overlap constraint: For each template $\mathbf{B}^{(t_{m,k})}_{X_{m,k}, S_{m,k}, A_{m,k}}$ centered at $X_{m,k}$, let D be the side length of its squared bounding box, then no other templates are allowed to be centered within a distance of ρD from $X_{m,k}$ (default setting: $\rho = .4$).

Such an assumption naturally leads to an inhibition step when we use a dictionary of templates to encode a training or testing image. Specifically, when a template is chosen to encode an image, this template will prevent overlapping templates from being selected. The template matching pursuit algorithm to be described below adopts such an inhibition scheme.

Connection with group Lasso. In the representation (3.4), each $\mathbf{B}^{(t_{m,k})}_{X_{m,k},S_{m,k},A_{m,k}}$ is a group of basis functions, and the K_m groups are to be selected from the collection of groups that correspond to all possible translated, rotated, scaled and deformed versions of the compositional patterns in the dictionary. The situation is very similar to that of group Lasso [38], which is also about selecting groups of variables from all possible groups. The selection by group Lasso is accomplished by solving a penalized least squares problem with a composite penalty based on the group structure. Our work goes beyond the group Lasso scenario in that the collection of groups is unknown, and we learn a dictionary of compositional patterns of these groups from training images. This dictionary then defines a large collection of groups by translation, rotation, scaling and deformation. Our work is a special case of structured sparsity. We call it compositional sparsity because we learn compositional patterns in sparse representations.

3.2. *Model complexity.* Before considering the learning algorithm that seeks to maximize the log-likelihood ratio (3.5), we need to resolve two issues regarding model complexity. One is how to choose the number of basis functions $n^{(t)}$ in each template $\mathbf{B}^{(t)}$ in the dictionary. The other is how to choose the number of templates T in the dictionary $\{\mathbf{B}^{(t)}, t = 1, ..., T\}$.

Determining the number of basis functions in a template in supervised learning. Suppose we are in the supervised learning setting where $\{\mathbf{I}_m, m = 1, ..., M\}$ are aligned image patches, and we want to learn an active basis template $\mathbf{B} = \{B_{x_i,s,\alpha_i}, i = 1, ..., n\}$. We employ the following penalized log-likelihood:

$$\sum_{m=1}^{M}\sum_{i=1}^{n}\left[\lambda_i h(\langle \mathbf{I}_m, B_{x_i+\Delta x_{m,i},s,\alpha_i+\Delta\alpha_{m,i}}\rangle) - \log Z(\lambda_i) - \gamma\right], \tag{3.6}$$

which is the sum of the log-likelihood ratio (2.10) and a penalty term $-\gamma$ associated with each basis function. There are two interpretations of γ. One is from the minimum description length (MDL) [30] perspective, where γ can be interpreted as the cost of coding the perturbations $(\Delta x_{m,i}, \Delta\alpha_{m,i})$ of B_{x_i,s,α_i} in the encoding of $\mathbf{I}_m$. Because there is a cost associated with each selected basis function B_{x_i,s,α_i}, the parameter γ encourages sparse or parsimonious model. The other interpretation is from the Bayesian information criterion (BIC) [31] perspective. From the Bayesian perspective, the perturbations $(\Delta x_{m,i}, \Delta\alpha_{m,i})$ should be integrated out according to their prior distributions, which are uniform distributions over the allowed ranges of perturbations. However, in our computation, the perturbations $(\Delta x_{m,i}, \Delta\alpha_{m,i})$ are inferred by local max pooling, i.e., they are actually maxed out instead of being integrated out. As a result, the resulting log-likelihood ratio with perturbations maxed out actually over-estimates the log-likelihood ratio with perturbations integrated out. The term γ may be considered an approximation to this over-estimation, which should be subtracted from the maxed-out log-likelihood.

In order to maximize the penalized log-likelihood ratio (3.6), we can continue to use the shared matching pursuit algorithm in subsection (2.5), except that we should stop the algorithm once the gain in the average log-likelihood ratio is smaller than γ, i.e.,

$$\lambda_i \sum_{m=1}^{M} h(\langle \mathbf{I}_m, B_{x_i+\Delta x_{m,i}, s, \alpha_i+\Delta\alpha_{m,i}}\rangle)/M - \log Z(\lambda_i) < \gamma.$$

This determines n. Currently we set the tuning parameter γ empirically at the default value of 1.

We can apply the above idea to unsupervised learning of the dictionary $\{\mathbf{B}^{(t)}, t = 1, ..., T\}$ from the non-aligned training images $\{\mathbf{I}_m\}$, by maximizing the penalized log-likelihood ratio

$$\sum_{m=1}^{M}\sum_{k=1}^{K_m}\left[l(\mathbf{I}_m \mid \mathbf{B}^{(t_{m,k})}_{X_{m,k},S_{m,k},A_{m,k}}) - n^{(t_{m,k})}\gamma\right], \tag{3.7}$$

where $n^{(t)}$ is the number of basis functions in $\mathbf{B}^{(t)}$.

Determining the number of templates. The number of templates T in the dictionary can be selected by an adjusted BIC criterion. The BIC criterion has been advocated by Fraley and Raftery (2002) [13] for determining the number of clusters in mixture models. Our model is similar to mixture models or clustering in the sense that the image patches are clustered into T different clusters. The difference is that these image patches are not independent examples, nor are they randomly cropped from the training images. Instead, they are to be cropped from the training images under the limited overlap constraint by a template matching pursuit algorithm to be described in the next subsection. From the clustering perspective, our method also bears some similarity to bi-clustering [24] or co-clustering, where in each cluster, different sets of basis functions are selected for representation. The difference is that these basis functions are not given variables. They need to be inferred from the image patches.

Recall that the BIC criterion is of the following form: maximized log-likelihood - number of parameters × log (number of training examples)/2. We can take (3.7) as the log-likelihood term, however, we have to correct for the overlap between the templates that encode the training images. The number of parameters in our model is $\sum_{t=1}^{T} n^{(t)}$, which is the number of basis functions in the templates in the dictionary. The number of training examples can be taken as $\sum_{m=1}^{M} K_m$, which is the number of image patches that are explained by the templates. So we define our adjusted BIC criterion as:

$$\beta\sum_{m=1}^{M}\sum_{k=1}^{K_m}\left[l(\mathbf{I}_m \mid \mathbf{B}^{(t_{m,k})}_{X_{m,k},S_{m,k},A_{m,k}}) - n^{(t_{m,k})}\gamma\right] - \frac{1}{2}\sum_{t=1}^{T} n^{(t)} \log \sum_{m=1}^{M} K_m, \tag{3.8}$$

where β is a ratio that discounts the overlap between the selected templates $\{\mathbf{B}^{(t_{m,k})}_{X_{m,k},S_{m,k},A_{m,k}}\}$. We define $\beta = n_1/n_2$. n_1 is the total number of pixels that are actually covered by the bounding boxes of these templates, where the overlapping pixels are only counted once. n_2 is the sum of the numbers of pixels within the bounding boxes of these templates, where a pixel is counted multiple times if it is covered by multiple templates. The reason we discount the overlap between the templates is that an image patch may be explained by multiple templates, which leads to inflated log-likelihood ratio. Since the BIC is a balance between the log-likelihood and the model complexity, we need to avoid such over-count for a fair BIC.

3.3. *Unsupervised learning algorithm.* There are two strategies for unsupervised learning.

Strategy 1: Sparsify and then compose. In order to discover the compositional patterns of basis functions in the sparse representations of the training images $\{\mathbf{I}_m\}$, it is tempting to first apply the plain matching pursuit or basis pursuit/Lasso to each training image $\mathbf{I}_m$ to obtain the sparse representation

$$\mathbf{I}_m = \sum_{i=1}^{n_m} c_{m,i} B_{x_{m,i}, s_{m,i}, \alpha_{m,i}} + U_m, \tag{3.9}$$

and then try to discover frequently occurring compositional patterns in the spatial grouping of the selected basis functions $\{B_{x_{m,i}, s_{m,i}, \alpha_{m,i}}, \forall i, m\}$. This was actually the strategy adopted by Zhu et al. [41] in their work on textons. The problem with such a sparsify-and-then-compose scheme is that the representation (3.9) produced by the matching pursuit or basis pursuit is an early decision or early commitment. Presumably, there may be many other representations that are no much less sparse than the representation (3.9), but they may be much more regular in terms of forming recurring compositional patterns. The results from matching pursuit or basis pursuit simply do not account for such uncertainty. In fact, even if the selected basis functions do form recurring patterns, discovering these patterns requires reasoning the correspondences between different groups that correspond to the same pattern. This is not an easy task, especially if the numbers of basis functions in the groups are not very small. The learning algorithm described below avoids such a sparsify-and-then-compose strategy. Not relying on early decision on sparse coding or edge detection is a key difference between our learning algorithm and those of [12] and [40].

Strategy 2: Iterative encoding and re-learning. Our learning algorithm seeks to maximize the penalized log-likelihood ratio (3.7) subject to the limited overlap constraint. It is an iterative algorithm where each iteration seeks to maximally increase the penalized log-likelihood ratio (3.7). Each iteration consists of two steps in the EM-style [7]: (I) Image encoding. Given the current dictionary $\{\mathbf{B}^{(t)}, t = 1, ..., T\}$, encode each training image $\mathbf{I}_m$ by translated, rotated, scaled and deformed versions of the templates in the dictionary, i.e., $\{\mathbf{B}^{(t_{m,k})}_{X_{m,k}, S_{m,k}, A_{m,k}}, k = 1, ..., K_m\}$. (II) Dictionary learning. Given the current encoding of $\mathbf{I}_m$ by $\{\mathbf{B}^{(t_{m,k})}_{X_{m,k}, S_{m,k}, A_{m,k}}, k = 1, ..., K_m\}$, re-learn each $\mathbf{B}^{(t)}$ from the image patches covered by the translated, rotated, scaled and deformed versions of the current $\mathbf{B}^{(t)}$, i.e., $\{\mathbf{B}^{(t_{m,k})}_{X_{m,k}, S_{m,k}, A_{m,k}}, t_{m,k} = t\}$.

To initialize the algorithm, we first learn the dictionary of active basis templates from randomly cropped image patches. Specifically, for each $\mathbf{B}^{(t)}$, we randomly cropped some image patches from training images, and then we learn $\mathbf{B}^{(t)}$ from these image patches using the shared matching pursuit algorithm described in subsection (2.5).

In the above learning process, we fix the total number of templates in the dictionary, T. We run the learning process for different values of T. Then we choose T that achieves the maximum of the adjusted BIC (3.8).

The following are the details of the two steps.

Step (I): Image encoding by template matching pursuit. Suppose we are given the current dictionary $\{\mathbf{B}^{(t)}, t = 1, ..., T\}$. Then for each $\mathbf{I}_m$, the template matching pursuit process seeks to represent $\mathbf{I}_m$ by sequentially selecting a small number of templates from the dictionary. Each selection seeks to maximally increase the penalized log-likelihood ratio (3.7).

[I.0] Initialize the maps of template matching scores for all (X, S, A, t):

$$\mathbf{R}_m^{(t)}(X, S, A) \leftarrow l(\mathbf{I}_m \mid \mathbf{B}_{X,S,A}^{(t)}) - n^{(t)}\gamma,$$

where $n^{(t)}$ is the number of basis functions in the t-th template in the dictionary and γ is a constant controling model complexity as explained above. This can be accomplished by first rotating the template $\mathbf{B}^{(t)}$ to orientation A, and then scanning the rotated template over the image zoomed to the resolution that corresponds to scale S. The larger the S is, the smaller the resolution is. Initialize $k \leftarrow 1$.

[I.1] Select the translated, rotated, scaled and deformed template by finding the global maximum of the response maps:

$$(X_{m,k}, S_{m,k}, A_{m,k}, t_{m,k}) = \arg \max_{X,S,A,t} \mathbf{R}_m^{(t)}(X, S, A).$$

[I.2] Let the selected arg-max template inhibit overlapping candidate templates to enforce limited overlap constraint. Let D be the side length of the bounding box of the selected template $\mathbf{B}_{X_{m,k},S_{m,k},A_{m,k}}^{(t_{m,k})}$, then for all (X, S, A, t), if X is within a distance ρD from $X_{m,k}$, then set the response $\mathbf{R}_m^{(t)}(X, S, A) \leftarrow -\infty$ (default setting: $\rho = .4$).

[I.3] Stop if all $\mathbf{R}_m^{(t)}(X, S, A, t) < 0$. Otherwise let $k \leftarrow k + 1$, and go to [I.1].

The template matching pursuit algorithm implements a hard inhibition to enforce the limited overlap constraint. In a more rigorous implementation, we may update the residual image by $U_m \leftarrow U_m - C_m \mathbf{B}_{X_{m,k},S_{m,k},A_{m,k}}^{(t_{m,k})}$ as in the original version of matching pursuit. But the current simplified version is more efficient.

The regularization parameter γ plays an important role in determining when to stop the template matching pursuit algorithm in the image encoding step (I). The response map $\mathbf{R}_m^{(t)}(X, S, A)$ is initialized as $l(\mathbf{I}_m \mid \mathbf{B}_{X,S,A}^{(t)}) - n^{(t)}\gamma$. If $l(\mathbf{I}_m \mid \mathbf{B}_{X,S,A}^{(t)}) < n^{(t)}\gamma$, then the gain in terms of the log-likelihood ratio does not compensate for the cost of coding the perturbations of the basis elements of the template. So we should stop the template matching pursuit if this is the case with all the remaining candidate templates.

The computation of the maps of template matching scores $\mathbf{R}_m^{(t)}(X, S, A)$ involves scanning the template $\mathbf{B}^{(t)}$ on the image $\mathbf{I}_m$ over all possible locations, orientations and scales. At each location X, scale S and orientation A, the computation of $\mathbf{R}_m^{(t)}(X, S, A)$ involves a linear combination of $n^{(t)}$ local maxima of Gabor filter responses, where $n^{(t)}$ is the number of basis functions in $\mathbf{B}^{(t)}$. The computational burden is about the same as computing Gabor filter responses at all possible locations, scales and orientations.

Step (II): Dictionary re-learning by shared matching pursuit. For each $t = 1, ..., T$, we re-learns $\mathbf{B}^{(t)}$ from all the image patches that are currently covered by $\mathbf{B}^{(t)}$. Each iteration of the shared matching pursuit process seeks to maximally increase the penalized log-likelihood ratio (3.7), given the current encoding $(t_{m,k}, X_{m,k}, S_{m,k}, A_{m,k}, k = 1, ..., K_m)$.

[II.0] Image patch cropping. For each $\mathbf{I}_m$, go through all the selected templates $\{\mathbf{B}^{(t_{m,k})}_{X_{m,k},S_{m,k},A_{m,k}}, \forall k\}$ that encode $\mathbf{I}_m$. If $t_{m,k} = t$, then crop the image patch of $\mathbf{I}_m$ (at the resolution that corresponds to $S_{m,k}$) covered by the bounding box of the template $\mathbf{B}^{(t_{m,k})}_{X_{m,k},S_{m,k},A_{m,k}}$.

[II.1] Template re-learning. Re-learn template $\mathbf{B}^{(t)}$ from all the image patches covered by $\mathbf{B}^{(t)}$ that are cropped in [II.0], with their bounding boxes aligned. The learning is accomplished by the shared matching pursuit algorithm of subsection (2.5).

Figure 7 illustrates the learning of maple leaf template from the training image shown in Figure 3. Figure 7.(a) traces the template of maple leaf learned over the first 7 iterations of the learning algorithm. (b) shows the process of shared matching pursuit for learning this template in the last (10th) iteration, where the constituent basis functions are sequentially added.

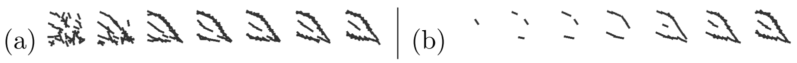

FIG. 7. (a) Template of leaf learned in the first 7 iterations of the unsupervised learning algorithm. (b) In each of iteration, the shared matching pursuit process selects wavelet elements sequentially to form each template. The sequence shows the process selecting 1, 3, 5, 10, 20, 30, 40 wavelets to form the leaf template in the last (10th) iteration.

This dictionary re-learning step re-learns each compositional pattern from the re-aligned raw image patches, where the sparse representations and the correspondences between the selected basis functions are obtained simultaneously by the shared matching pursuit algorithm, thus avoiding the difficulty faced by the sparsify-and-then-compose procedure of Strategy I.

Random initialization and polarization. The learning algorithm is initialized by learning from image patches randomly cropped from the training images. As a result, the initially learned templates are rather meaningless, but meaningful templates emerge very quickly after a few iterations. See Figure 7.(a) for an illustration.

During the template matching pursuit process of the first iteration, we continue to select templates even if the template matching scores are below zero. We stop the template matching pursuit process for each $\mathbf{I}_m$ when all the candidate templates are inhibited on $\mathbf{I}_m$. That is because the initial templates in the dictionary are rather random, so we force them to explain the whole image of $\mathbf{I}_m$ even if the templates do not match the image well.

In the beginning, the differences among the initial templates are small. However, as the algorithm proceeds, the small differences among the initial templates trigger a polarizing or specializing process, so that the templates become more and more different, and they specialize in encoding different types of image patches. One may start the algorithm multiple times and select the dictionary that achieves the maximum of the log-likelihood ratio (3.7).

3.4. *Notes on the learning algorithm.* This subsection consists of some notes on various subtle aspects of the learning algorithm. More practically minded readers can jump to the next section for experimental results.

Generalized matching pursuit in both steps. Both the image encoding step (I) and the dictionary re-learning step (II) are generalizations of the matching pursuit algorithm. In fact, the whole learning algorithm can be viewed as an encoding algorithm, which seeks to automatically discover the frequently occurring compositional patterns of the selected basis functions that are otherwise overlooked by the plain matching pursuit algorithm. In other words, the algorithm seeks to find a highly patterned sparse coding, where the selected basis elements are not only sparse but they also form recurring patterns in their spatial arrangements. The re-learning of each template can be viewed as encoding multiple image patches by a single template, thus resulting in more efficient encoding than the plain matching pursuit algorithm.

Relationship with sparse component analysis and K-SVD. As our model is a recursion of the Olshausen-Field model, our learning algorithm can also be viewed as a recursion of the learning scheme of Olshausen and Field, which is sometimes called sparse component analysis in the literature. In the Olshausen-Field model $\mathbf{I}_m = \sum_{i=1}^N c_{m,i} B_i + U_m$, the dictionary of $(B_i, i = 1, ..., N)$ is learned from the training image patches $\{\mathbf{I}_m\}$ by minimizing

$$\sum_{m=1}^{M} \left[\|\mathbf{I}_m - \sum_{i=1}^{N} c_{m,i} B_i\|^2 + \lambda \sum_{i=1}^{N} S(c_{m,i}) \right], \tag{3.10}$$

over both $(c_{m,i})$ and (B_i), where $S()$ is a sparsity inducing penalty function, and λ is the regularization parameter. The learning algorithm iterates the following two steps. (I) Image encoding. For each $\mathbf{I}_m$, update $(c_{m,i}, \forall i)$ given $(B_i, \forall i)$. (II) Dictionary learning. Update (B_i) given $(c_{m,i}, \forall i, m)$. In Olshausen-Field learning algorithm, both steps are carried out by gradient descent. In a related learning algorithm called K-SVD [1], (I) can be accomplished by any pursuit algorithm such as matching pursuit or basis pursuit, and (II) is accomplished by SVD. Our algorithm is even more similar to K-SVD than to the Olshausen-Field algorithm. It is interesting to notice that in both K-SVD and our algorithm, the updating of each representational unit in step (II) is performed only on the image patches where this representational unit is currently active, i.e., the representational unit is re-learned from image patches that is currently encoded by this unit. Also similar to K-SVD, in our algorithm, the coefficients and the basis functions are updated together in dictionary re-learning in step (II).

Non-convex objective function. One complication about our learning method is that the negative log-likelihood ratio is not convex, and our learning algorithm is a greedy algorithm that is similar to the EM algorithm [7]. In fact, this is also the case with the objective function (3.10) in Olshausen-Field sparse component analysis, which is non-convex in the joint domain of the unknown basis functions and their coefficients. This is the case with many other unsupervised learning methods as well.

Linear subtraction versus occlusion. In both the template matching pursuit in step (I) and the shared matching pursuit in step (II), the explaining-away inhibition is carried out by hard inhibition that enforces limited overlap between templates in step (I) and the approximated non-overlap between basis functions in step (II). Such hard inhibition amounts to occlusion, where a selected template or basis function occludes nearby overlapping templates or basis functions. A more rigorous explaining-away mechanism in the context of linear additive structures (2.4) and (3.4) is by linear subtraction, where a selected template (group of basis functions) or a selected basis function is linearly subtracted from the training images, see (2.7), so that other templates or basis functions continue to explain the residual images. This linear subtraction scheme can be more computationally demanding than hard inhibition.

Matching pursuit versus penalized least squares. Both steps (I) and (II) in our learning algorithm are generalizations of matching pursuit, and both can be replaced by generalizations of basis pursuit or Lasso. Step (I) can be replaced by group Lasso, where the groups are the groups of basis functions that correspond to all possible translated, rotated, scaled and deformed versions of the templates in the current dictionary. Step (II) can be replaced by a different type of group Lasso, where the groups are formed across the aligned image patches from which we re-learn the template. Specifically, we group the coefficients of the same basis functions (up to local perturbations) across the aligned image patches, so that we always select the same set of basis functions for these aligned image patches. This is sometimes called multi-task learning [20] or support union recovery in multivariate regression [25]. Such penalized least squares schemes can be much more expensive computationally than the corresponding versions of matching pursuit.

4. Experiments.

This section presents experiments based on the unsupervised learning algorithm in the previous section. The data and code for reproducing the experimental results reported in this paper can be downloaded from the project page [1].

4.1. *Image representation.* In order to learn the dictionaries of compositional patterns from training images, we run the algorithm for 10 iterations. We set $n^{(t)}$ to be a fixed value (default setting: 40) in the first 9 iterations. In the last iteration, we choose $n^{(t)}$ using the method described in subsection (3.2), and we use the templates with adaptively chosen $n^{(t)}$ to represent the training images.

Figure 8 shows an example of selecting the number of templates T in the dictionary. In each row, the first image is the training image. The remaining four blocks display the learned dictionaries of compositional patterns of basis functions in the form of active basis templates, as well as the representations of the training images using the learned dictionaries. The numbers of templates in the dictionaries are respectively 1, 2, 3, and 4. It takes about 10 seconds on a current desktop to learn a dictionary for the first image, which is of size 480 × 768, and the running times for the other images are similar. Just as in Figures 3 and 7, each basis function or wavelet is illustrated by a bar at the same location and orientation, and with the same length as the corresponding wavelet. All the templates are of the size 100 × 100. We also display the adjusted BIC criterion for each learned dictionary. The learned dictionaries are quite meaningful, and they give meaningful representations of the training images. It is interesting to observe how the dictionaries with only 1 template strive to represent the images.

[1] http://www.stat.ucla.edu/∼ywu/ABC/ABC.html

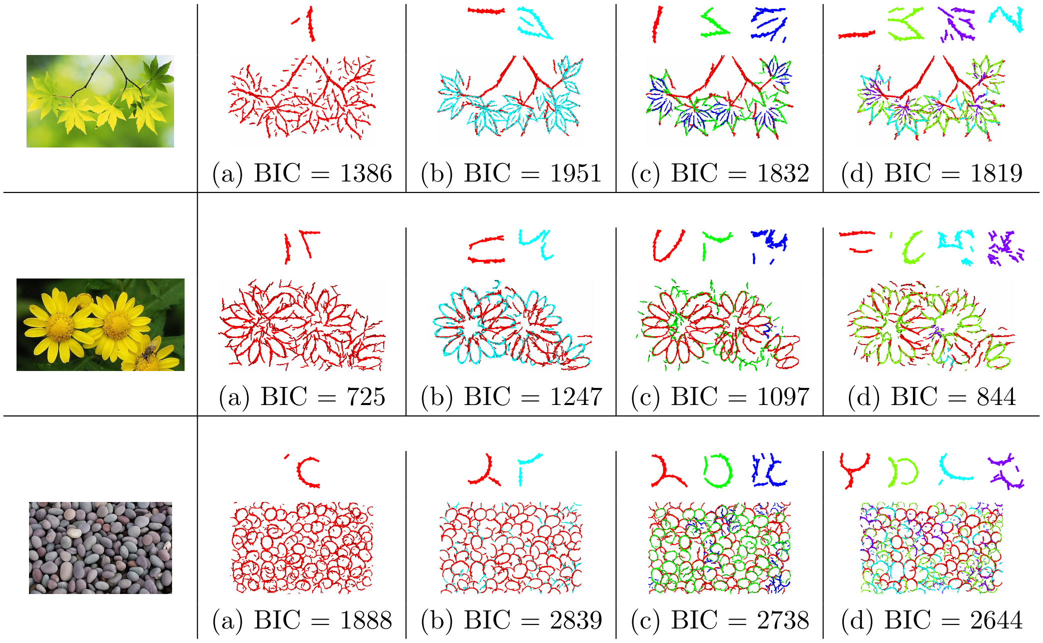

(a) BIC = 1386 (b) BIC = 1951 (c) BIC = 1832 (d) BIC = 1819

(a) BIC = 725 (b) BIC = 1247 (c) BIC = 1097 (d) BIC = 844

(a) BIC = 1888 (b) BIC = 2839 (c) BIC = 2738 (d) BIC = 2644

FIG. 8. The adjusted BIC computed for different numbers of templates (1-4) in the dictionaries. The size of templates is 100 × 100. The allowed range of scale change is $\{.8, 1, 1.2\}$ of the original image. The templates are allowed full range of rotation. The maximal number of basis functions in each template is 40 and the actual number is automatically determined.

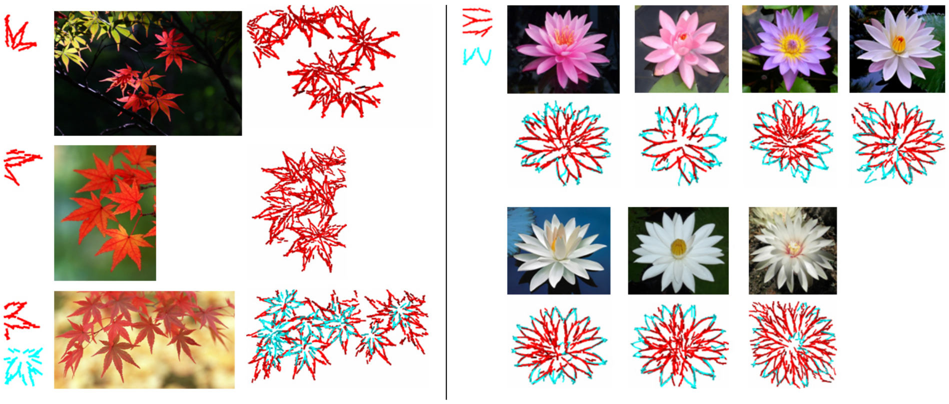

FIG. 9. Maple leaves and lotus. Parameter setting is the same as in Figure 8.

As to the issue of selecting image resolution, for the example of maple leaves, we also learn dictionaries of templates at different resolutions of the training image. The resolution in Figure 8.(b) achieves the maximum BIC per pixel. This is essentially equivalent to determining the size of templates. However, we feel that instead of selecting

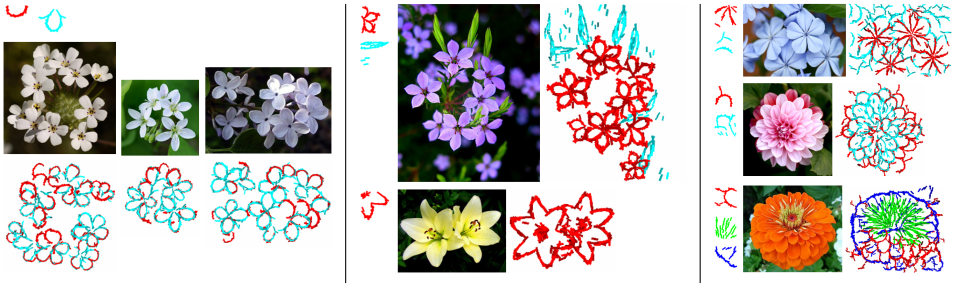

Fig. 10. Flowers. Parameter setting is the same as in Figure 8. For the two examples in the middle, the templates consist of more than one petal. This is due to the fact that the templates are of a squared shape and are relatively large.

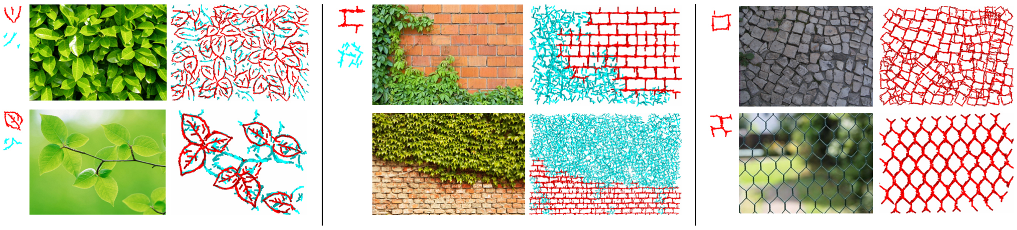

Fig. 11. Ivy, leaves, ivy wall, pavement, and fence. Parameter setting is the same as in Figure 8. For the ivy wall example, the bottom row contains the testing image and its representation by the dictionary learned from the training image on the top row.

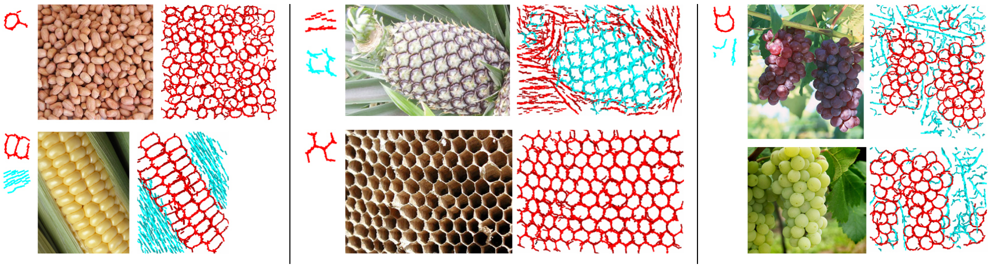

Fig. 12. Peanuts, corn, pineapple, beehives, and grape. Parameter setting is the same as in Figure 8. For the grape example, the bottom row contains the testing image and its representation by the dictionary learned from the training image on the top row.

the optimal resolution, it may be more appropriate to learn dictionaries at multiple resolutions or scales and combine them for image representation and understanding, just like the multi-resolution analysis in wavelets theory.

The adjusted BIC is useful for determining the number of compositional patterns in the dictionary. However, it may be more appropriate to use it to determine the rough range of possible numbers of patterns, instead of using it to pinpoint the exact number. For instance, in the maple leaves example, the dictionary with 3 patterns also give a

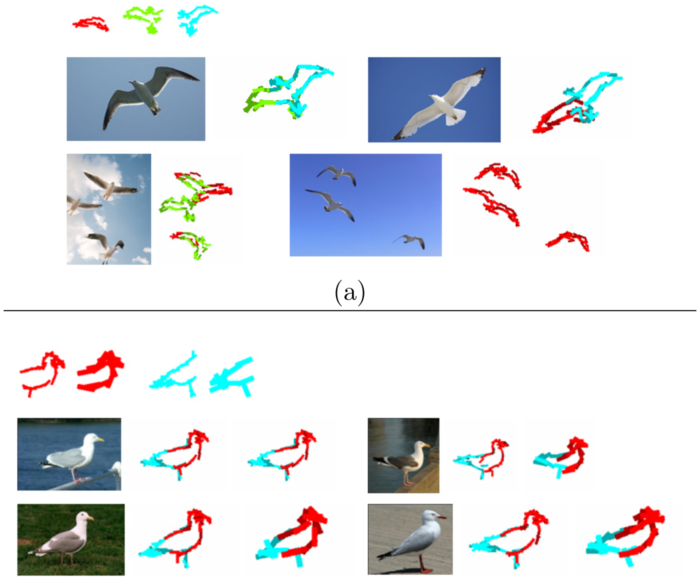

(a)

(b)

Fig. 13. Seagulls flying (number of training images is 20) and standing (number of training images is 11). For the standing seagulls experiment, we learn multi-scale templates at two different scales (the scale parameters are .7 and 1.4 respectively). We sum the log-likelihood scores of the templates at the two scales in order to compute the template matching scores in the template matching pursuit process.

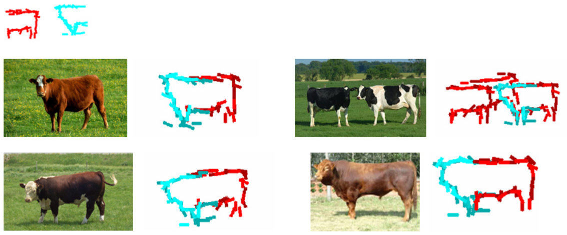

Fig. 14. Cattle (number of training images is 17). Parameter setting is the same as in Figure 8 except that the allowed range of template rotation is $\{-2, -1, 0, 1, 2\} \times \pi/16$.

very meaningful representation of the training image. For applications such as image classification, the number of patterns in the dictionary may be determined by cross validation instead of BIC.

Figures 9 to 17 show more examples of representing natural images. In some of the images, such as flowers, leaves and brick wall, the compositional patterns repeat themselves within the same image. For some other images, such as animal bodies and

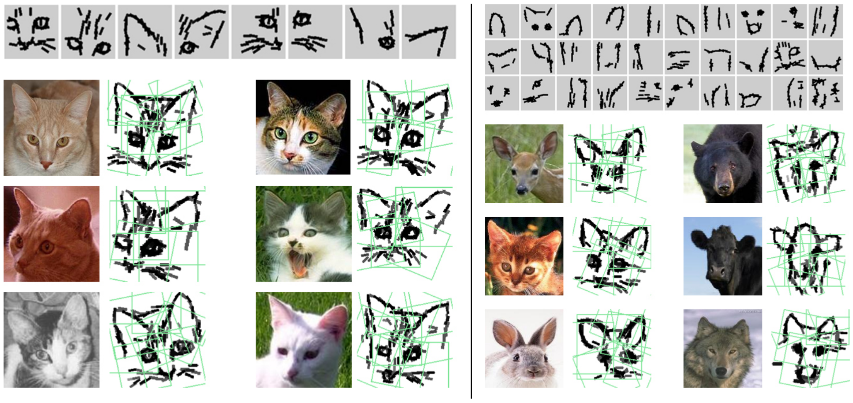

FIG. 15. Cat faces (number of training images is 89) and animal faces (number of training images is 490). Parameter setting is the same as in Figure 14.

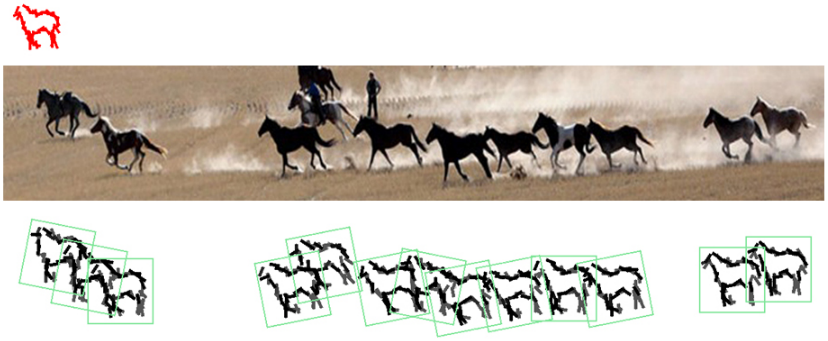

FIG. 16. Horse. Parameter setting is the same as in Figure 8, except that the allowed range of rotation of the template is $\{-1, 0, 1\} \times \pi/16$.

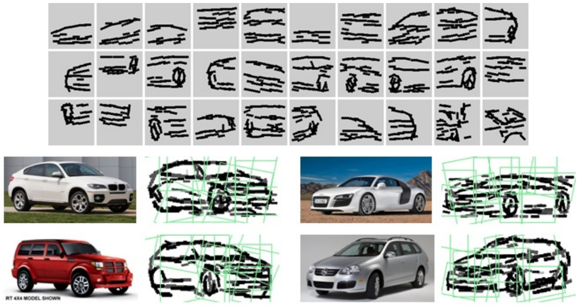

FIG. 17. Cars. Parameter setting is the same as in Figure 14. Number of training images is 245.

faces, the compositional patterns repeat across different images. For these images, the learning algorithm does not assume that the images are aligned.

In the dictionary re-learning step (II), for each entry in the dictionary, we can learn a multi-scale template from the aligned image patches using wavelets at multiple scales. A multi-scale template has multiple component templates, each consisting of wavelets at a single scale. If the gaps between the scales of the wavelets are sufficiently large, then templates of different scales can be considered independent. Therefore, the learning of each component template can be done separately at each scale, and in the image encoding step (I), for each entry in the dictionary, we can combine the log-likelihood scores of the component templates at multiple scales in order to compute the overall template matching scores. See the standing seagulls experiment in Figure 13 for an illustration.

4.2. *Better "words" for image classification.* The learned compositional patterns can be used as "words" in the bag-of-word method for image classification. Let $\{\mathbf{B}^{(t)}, t = 1, ..., T\}$ be the templates learned from positive training images. For each image $\mathbf{I}_m$, let $\mathbf{R}_m^{(t)}(X, S, A) = l(\mathbf{I}_m \mid \mathbf{B}_{X,S,A}^{(t)})$ be the log-likelihood score of $\mathbf{B}^{(t)}$ at location X, scale $S \in \{.8, 1, 1.2\}$ and orientation $A \in \{\pm 1, 0\} \times \pi/16$ (see subsection (3.1) and Equation (3.2)). Let $r_m^{(t)}(A) = \max(\max_{X,S} \mathbf{R}_m^{(t)}(X, S, A), 0)$ be the maximum score (lower-bounded by 0) at orientation A. Then for each $\mathbf{I}_m$, we have a $3T$-dimensional feature vector $(r_m^{(t)}(A), t = 1, ..., T, \forall A)$ (the factor 3 is due to the fact that we keep the scores of all the 3 orientations). We then train a linear logistic regression on such $3T$-dimensional feature vectors (regularized by ℓ_2 norm [9]) for image classification.

Table 1. Accuracies (%) on binary classification tasks for 24 categories from Caltech-101, ETHZ Shape and Graz-02 data sets.

Datasets	SIFT+SVM	Our method	Datasets	SIFT+SVM	Our method
Watch	90.1 ± 1.0	91.3 ± 2.0	Sunflower	76.0 ± 2.5	92.9 ± 2.5
Laptop	73.5 ± 5.3	87.9 ± 2.2	Chair	62.5 ± 5.0	89.1 ± 1.1
Piano	84.5 ± 4.2	93.4 ± 3.0	Lamp	61.5 ± 4.5	81.7 ± 3.7
Ketch	82.2 ± 0.8	89.2 ± 2.4	Dragonfly	66.0 ± 4.0	87.0 ± 4.1
Motorbike	93.9 ± 1.2	93.7 ± 0.9	Umbrella	73.4 ± 4.4	89.3 ± 2.5
Guitar	70.0 ± 2.4	80.9 ± 5.1	Cellphone	68.7 ± 5.1	87.9 ± 4.2
Schooner	64.3 ± 2.2	93.8 ± 2.7	Face	91.8 ± 2.3	95.8 ± 2.8
Ibis	67.8 ± 6.0	83.0 ± 1.9	Starfish	73.1 ± 6.7	85.3 ± 4.7
ETHZ-Bottle	68.6 ± 3.2	76.1 ± 3.3	ETHZ-Cup	66.0 ± 3.3	67.5 ± 4.4
ETHZ-Swans	64.2 ± 1.5	82.4 ± 0.5	ETHZ-Giraffes	61.5 ± 6.4	71.5 ± 3.5
ETHZ-Apple	55.0 ± 1.8	68.3 ± 5.2	Graz02-Person	70.4 ± 1.2	73.8 ± 2.3
Graz02-Car	64.0 ± 6.7	63.5 ± 5.1	Graz02-Bike	68.5 ± 2.8	77.6 ± 2.3

We evaluate this simple classifier on 16 categories from Caltech-101 [10], all ETHZ Shape [11] and all Graz-02 [23] data sets, where we test it on binary classification task. We resize all images to 150^2 pixels while maintaining their aspect ratios. We randomly sample 30 positive and negative images respectively as training data, and leave the rest as testing data. For Caltech-101 and Graz-02, negative images are from background category. For ETHZ, negative examples are from images other than the target category. For each category, we learn a dictionary of $T = 10$ templates. Each is of the size 100×100 with $n = 30$ basis functions.

As a comparison, for each image, we densely extract SIFT features [21] with patch size 16×16 and step size 8, from both positive and negative images. We then quantize them into 50, 100 and 500 words respectively by k-means clustering [5] and feed them into SVM [34, 2] (linear and histogram intersection kernel [17]). We take the best of these 6 results (3 numbers of words (50, 100, 500) × 2 types of SVM (linear, kernel)) and compare it with our method. All experiments are carried out with 5 independent runs and the 95% confident intervals on accuracies are calculated. Table 1 presents the results. It shows that our method generally outperforms the popular SIFT + SVM method even though our method uses a much smaller dictionary of words (10 in our method versus 50, 100, or 500 in SIFT + SVM).

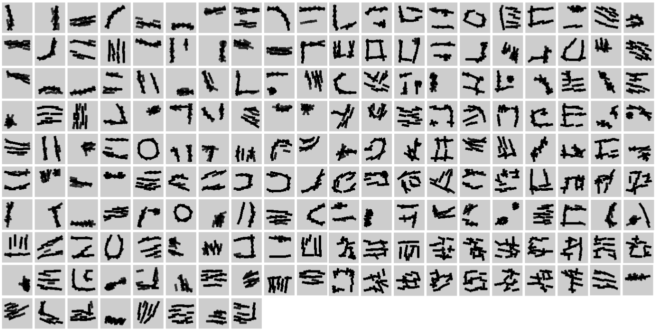

FIG. 18. Learned dictionary of templates from the Caltech-101 dataset in one run of an experiment, with 30 training images from each category. Template size is 64×64. Number of basis functions in each template is 15.

We also test our method on the whole Caltech-101 data set. We learn $T = 200$ templates from the training images from all the 101 categories together. In one set of experiments, 15 training images are randomly sampled from each category in each run. In another set of experiments, 30 training images are randomly taken from each category in each run. In each set of experiments, 5 runs are repeated.

Each template is of the size 64×64 with $n = 15$ basis functions. During the learning algorithm, if the number of image patches encoded by a template is less than a threshold, then this template is eliminated from the dictionary. For 15 training images per category, the threshold is set at 5. For 30 training images per category, the threshold is set at 10. Figure 18 displays the learned dictionary of templates in one run of experiment with 30 training images per category. They seem to capture the mid-level structures such as lines, corners and circles etc.

For each image $\mathbf{I}_m$, and for each template $\mathbf{B}^{(t)}$ at each orientation A, besides the global maximum $r_m^{(t)}(A)$, we also divide $\mathbf{I}_m$ equally into 2×2 sub-regions and take the maximum within each sub-region. In addition to each maximum, we also take the corresponding average. So each $\mathbf{B}^{(t)}$ extracts 30 features from $\mathbf{I}_m$. Thus in total, each $\mathbf{I}_m$ produces a

$30T$-dimensional feature vector. We adopt standard evaluation protocol. For 15 training images per category, the accuracy of our method is $61.6 \pm 2.2\%$ (compared to $57.7 \pm 1.5\%$ in [18]). For 30 training images per category, our result is $68.5 \pm 0.9\%$ (compared to $65.4 \pm 0.5\%$ in [18]). While more recent papers such as [39] and the references therein report better performances based on spatial pyramid matching [17], we do not use k-means to further cluster response maps into another layer of codewords, neither do we use any kernel.

5. Discussion. In this section, we first discuss the contributions and limitations of our current work. Then we shall compare our work with related work in the literature.

5.1. *Contributions and limitations.* The main contribution of this paper to propose a framework for learning compositional sparse code for representing natural images. We propose a representational scheme based on composite representational units, which are groups of basis functions of frequently occurring compositional patterns. We have developed an unsupervised learning algorithm for learning dictionaries of compositional patterns from training images, where the compositional patterns arise from seeking commonly shared sparse coding of image patches. Our experiments on natural images of plants and animals etc. show that our method is capable of learning meaningful compositional patterns, which lead to meaningful representations of training and testing images.

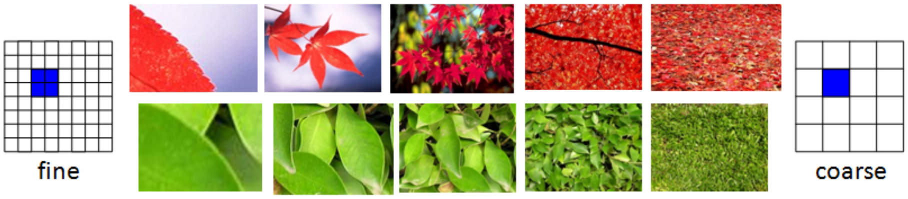

Fig. 19. Image scaling and regimes of patterns: As we zoom out the images, the patterns undergo a transition from low-entropy regime of geometric structures to mid-entropy regime of object shapes to high-entropy regime of stochastic textures. Our current method targets the mid-entropy regime of shape patterns.

In terms of biological plausibility, the Olshausen-Field model is a model for simple V1 cells. The local max pooling of Riesenhuber and Poggio [29] and the arg-max retrieval and inhibition of the active basis model may be related to complex V1 cells. The dictionaries of active basis templates learned by our method may be related to V2 cells and beyond.

The following are limitations of our work. First, as illustrated by Figure 19, as we zoom out the images, the image patterns undergo a transition from low-entropy regime of geometric structures to mid-entropy regime of object shapes to high-entropy regime of stochastic textures [36] (patterns such as the brick wall are also textures, but they are structural textures instead of stochastic textures). Our current model mainly targets the mid-entropy regime of object shapes and textons. It does not account for stochastic texture patterns or appearance patterns that are ubiquitous in natural scenes. The current model does not account for flatness patterns that are prominent in the low-entropy regime either. Perhaps one may entertain a Markov random field model of the form

$$p(\mathbf{I}) = \frac{1}{Z(\Lambda)} \exp\{\sum_{x,s,\alpha} \lambda_{x,s,\alpha}(h(|\langle \mathbf{I}, B_{x,s,\alpha}\rangle|^2))\}q(\mathbf{I}),$$

for the distribution of the nominal template (before shape deformation), where $\lambda_{x,s,\alpha}$ can be either positive (for sketch patterns) or negative (for flatness patterns). One can sparsify $\lambda_{x,s,\alpha}$ by ℓ_1 penalized maximum likelihood. For homogeneous $\lambda_{x,s,\alpha}$, i.e., $\lambda_{x,s,\alpha}$ is independent of x within a local neighborhood, then $p(\mathbf{I})$ becomes the FRAME (filter, random field, and maximum entropy) model for textures [43]. Although $p(\mathbf{I})$ seems to encompass sketch patterns, flatness patterns and stochastic texture patterns, fitting $p(\mathbf{I})$ in general requires MCMC simulation, which can be expensive. The active basis model that assumes approximate orthogonality of the selected basis functions and the independence of their coefficients may be considered an efficient approximation of the sketch components of $p(\mathbf{I})$.

Another limitation is that the model is still not a fully generative model because we have not modeled the spatial arrangements of the templates. A third limitation is that we assume that the dictionary of the basis functions are given as Gabor wavelets. It is desirable to learn these basis functions from training images.

The active basis models are currently learned by generative approach based on likelihood. It may be possible to learn the models discriminatively by regularized logistic regression after bringing in negative image patches.

5.2. *Relations with hierarchical models. AND-OR grammar.* Our work connects the sparsity principle to compositionality principle [15, 42, 16], which holds that the visual patterns are hierarchical compositions of constituent parts. In particular, in the language of AND-OR grammar of Zhu and Mumford (2006) [42], the dictionary of the active basis templates can be considered a big OR node, where each template is a child node of this OR node, and each template is itself an AND-OR structure, where AND means composition of the constituent basis functions, and OR means perturbations of the locations and orientations of the basis functions, as well as variations of their coefficients. The OR-variations make the composite units invariant to these variations, so that the composite units are more abstract and generalizable.

In terms of composing Gabor wavelets, our representation is similar to that of [12] as well as [40]. The difference is that, our method is based on a top-down generative model, where the compositional patterns are re-learned in each iteration of the learning algorithm from raw image patches by seeking to maximize the log-likelihood ratio.

Our method may be extended to learn multi-layer compositional sparse coding models, where each template is a deformable composition of part-templates, and each part-template itself is a deformable composition of a number of basis functions, i.e., each part-template is an active basis model, so the whole template may be called a hierarchical active basis model. Figure 20 illustrates the basic idea of such hierarchical active basis models in the setting of supervised learning, where the objects in the images are roughly aligned. In order to learn a hierarchical active baiss model, we can first learn a collection of highly overlapping part-templates, where each part-template is allowed to

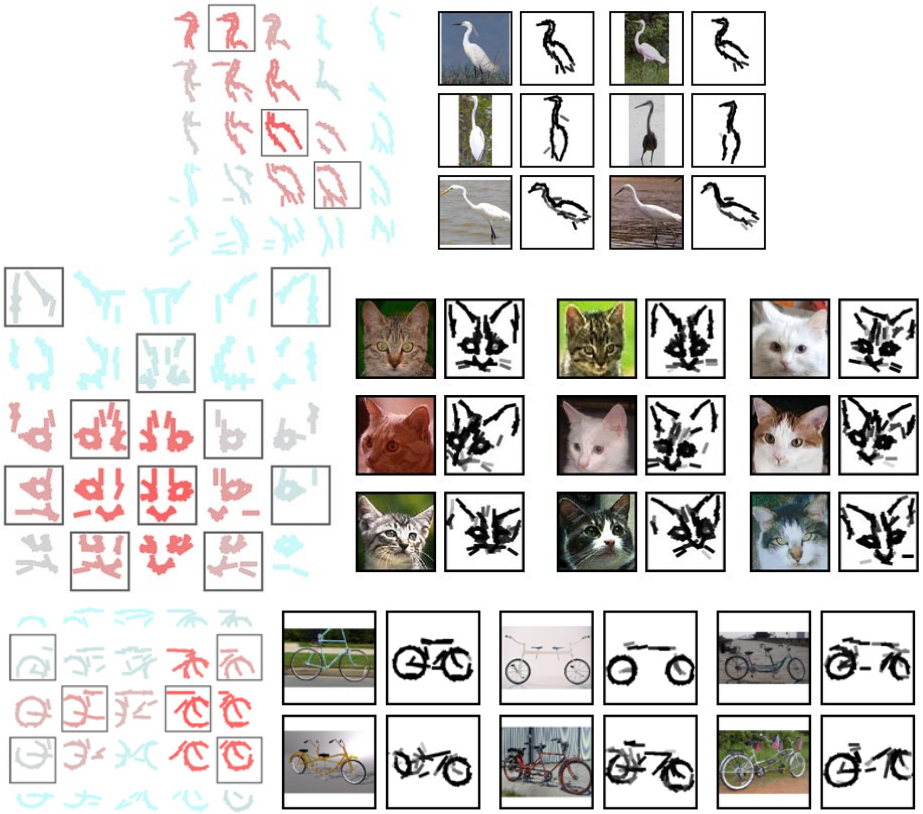

FIG. 20. Supervised learning of hierarchical active basis models. We first learn overlapping part-templates, and then select some of them (with bounding boxes) according to their log-likelihood scores (indexed by color). The learned models are deformable compositions of active basis models.

move within a local range, to account for shape deformation. Then we pursue a small number of part-templates according to their log-likelihood scores (indexed by color in Figure 20) to enforce that the selected part-templates only have limited overlap. We may use such hierarchical active basis models as our representational units, and we may learn a dictionary of such hierarchical active basis models in unsupervised setting. The recent paper by Si and Zhu (2013) [35] explores the learning of And-Or templates which include the hierarchical active basis models as special cases.

Deep learning. Our work is related to deep learning with sparsity constraint [18, 39]. The difference is that our representational units are sparse compositions of automatically selected basis functions, where sparsity is explicitly built into the representational units by the shared matching pursuit process. The representational units are no longer linear basis functions on top of the wavelets coefficients or filter responses at the lower layer. Also, our model is not built on a pre-processed sparse representation, which, as we have argued in strategy I of subsection (3.3), amounts to early decision. In our learning algorithm, each iteration re-learns each template from raw image patches, where the sparse representations, their correspondences, and the template are obtained simultaneously instead of being obtained one after another.

HMAX model. Our work is related to the HMAX model of [29]. The local max pooling is employed for inferring the perturbations of the wavelet elements of the active basis model. In HMAX, the dictionary of the second layer consists of maps of local max pooling of Gabor responses. In our work, we explicitly learn the recurring compositional patterns of the wavelets guided by a generative model.

Acknowledgement. We thank the two anonymous reviewers for their detailed and insightful comments and suggestions that have helped us improve the presentation of this work. The work reported in this article is supported by NSF DMS 1007889, NSF IIS 1018715, ONR N00014-10-1-0933, and DARPA N00014-10-1-0933.

References

[1] M. Aharon, M. Elad, and A.M. Bruckstein. The K-SVD: an algorithm for designing of overcomplete dictionaries for sparse representation, *IEEE Transactions On Signal Processing*, **54**, 4311-4322, 2006.

[2] C. C. Chang and C. J. Lin. LIBSVM: A library for support vector machines. *ACM Transactions on Intelligent Systems and Technology*, **2**, 1-27, 2011.

[3] S. Chen, D. Donoho, and M. A. Saunders. Atomic decomposition by basis pursuit. *SIAM Journal on Scientific Computing*, **20**, 33-61, 1999.

[4] J. Chen and X. Huo. Sparse representations for multiple measurements vectors (mmv) in an overcomplete dictionary. *Proceedings of IEEE International Conference on Acoustics, Speech, and Signal Processing*, **4**, 257260, 2005.

[5] G. Csurka, C. Dance, L. Fan, J. Willamowski, and C. Bray. Visual categorization with bags of keypoints. *Workshop of European Conference on Computer Vision*, 2004.

[6] J. Daugman. Uncertainty relation for resolution in space, spatial frequency, and orientation optimized by two-dimensional visual cortical filters. *Journal of Optical Society of America*, **2**, 1160-1169, 1985.

[7] A. P. Dempster, N. M. Laird, and D. B. Rubin. Maximum likelihood from incomplete data via the EM algorithm (with discussion). *Journal of the Royal Statistical Society, B*, **39**, 1-38, 1977.

[8] D. L. Donoho and X. Huo. Uncertainty principles and ideal atomic decomposition. *IEEE Transactions on Information Theory*, **47**, 2845-62, 2001.

[9] R. E. Fan, K. W. Chang, C. J. Hsieh, X. R. Wang, and C. J. Lin. LIBLINEAR: A library for large linear classification. *Journal of Machine Learning Research*, **9**, 1871-1874, 2008.

[10] L. Fei-Fei, R. Fergus, and P. Perona. Learning generative visual models from few training examples: an incremental Bayesian approach tested on 101 object categories. *CVPR Workshop*, 2004.

[11] V. Ferrari, F. Jurie and C. Schmid. From images to shape models for object detection. *International Journal of Computer Vision*, **87**, 284–303, 2010.

[12] S. Fidler, M. Boben, and A. Leonardis. Similarity-based cross-layered hierarchical representation for object categorization. *IEEE Conference on Computer Vision and Pattern Recognition*, 2008.

[13] C. Fraley and A. E. Raftery. Model-based clustering, discriminant analysis, and density estimation. *Journal of the American Statistical Association*, **97**, 611-631, 2002.

[14] J. H. Friedman. Exploratory projection pursuit. *Journal of the American Statistical Association*, **82**, 249-266, 1987.

[15] S. Geman, D. F. Potter, and Z. Chi. Composition systems. *Quarterly of Applied Mathematics*, **60**, 707–736, 2002.

[16] Y. Jin and S. Geman. Context and hierarchy in a probabilistic image model. *IEEE Conference on Computer Vision and Pattern Recognition*, 2006.

[17] S. Lazebnik, C. Schmid, and J. Ponce. Beyond bags of features: spatial pyramid matching for recognizing natural scene categories. *IEEE Conference on Computer Vision and Pattern Recognition*, 2006.

[18] H. Lee, R. Grosse, R. Ranganath, and A. Y. Ng. Convolutional deep belief networks for scalable unsupervised learning of hierarchical representations. *International Conference on Machine Learning*, 2009.

[19] C. Lo, *Amazing Chinese Characters*, Panda Media Co., 2002.

[20] K. Lounici, A. B. Tsybakov, M. Pontil, and S. A. van de Geer. Taking advantage of sparsity in multi-task learning. *Proceedings of the 22nd Conference on Learning Theory*, 2009

[21] D. Lowe. Distinctive image features from scale-invariant keypoints. *International Journal of Computer Vision*, **60**, 91–110, 2004.

[22] S. Mallat and Z. Zhang. Matching pursuit in a time-frequency dictionary. *IEEE Transactions on Signal Processing*, **41**, 3397-3415, 1993.

[23] M. Marszalek and C. Schmid. Accurate object localization with shape masks. *IEEE Conference on Computer Vision and Pattern Recognition*, 2007.

[24] B. Mirkin. *Mathematical Classification and Clustering.* Kluwer Academic Publishers, 1996.

[25] G. Obozinski, M. J. Wainwright, and M. I. Jordan, Support union recovery in high-dimensional multivariate regression, *Annals of Statistics*, **39**, 1-47, 2011.

[26] B. A. Olshausen and D. J. Field. Emergence of simple-cell receptive field properties by learning a sparse code for natural images. *Nature*, **381**, 607-609, 1996.

[27] B. A. Olshausen, P. Sallee and M. S. Lewicki. Learning sparse image codes using a wavelet pyramid architecture. *Advances in Neural Information Processing Systems*, **13**, 887-893, 2001.

[28] S. D. Pietra, V. D. Pietra, J. Lafferty. Inducing Features of Random Fields *IEEE Transactions on Pattern Recognition and Machine Intelligence*, **19**, 380-393, 1997

[29] M. Riesenhuber and T. Poggio. Hierarchical models of object recognition in cortex. *Nature Neuroscience*, **2**, 1019–1025, 1999.

[30] J. Rissanen. *Information and Complexity in Statistical Modeling.* Springer, 2007.

[31] G. E. Schwarz. Estimating the dimension of a model. *Annals of Statistics*, **6**, 461-464, 1978.

[32] J. Tropp, A. Gilbert, and M. Straus. Algorithms for simultaneous sparse approximation. part I: Greedy pursuit. *Journal of Signal Processing*, **86**, 572588, 2006.

[33] R. Tibshirani. Regression shrinkage and selection via the lasso. *Journal of the Royal Statistical Society, B*, **58**, 267-288, 1996.

[34] V. N. Vapnik. *The nature of Statistical Learning Theory.* Springer, 2000.

[35] Z. Si and S.C. Zhu. Learning and-or templates for object modeling and recognition. *IEEE Transactions on Pattern Analysis and Machine Intelligence*, to appear, 2013.

[36] Y. N. Wu, C. Guo, and S. C. Zhu. From information scaling of natural images to regimes of statistical models. *Quarterly of Applied Mathematics*, **66**, 81-122, 2008.

[37] Y. N. Wu, Z. Si, H. Gong, and S. C. Zhu. Learning active basis model for object detection and recognition. *International Journal of Computer Vision*, **90**, 198-235, 2010.

[38] M. Yuan and Y. Lin. Model selection and estimation in regression with grouped variables. *Journal of the Royal Statistical Society, B*, **68**, 49-67, 2006.

[39] M. Zeiler, G. Taylor and R. Fergus. Adaptive deconvolutional networks for mid and high level feature learning. *International Conference on Computer Vision*, 2011.

[40] L. Zhu, C. Lin, H. Huang, Y. Chen, and A. Yuille. Unsupervised structure learning: hierarchical recursive composition, suspicious coincidence and competitive exclusion. *European Conference on Computer Vision*, 2008.

[41] S. C. Zhu, C. Guo, Y. Wang, and Z. Xu. What are textons? *International Conference on Computer Vision*, **62**, 121–143, 2005

[42] S. C. Zhu and D. B. Mumford. A stochastic grammar of images. *Foundations and Trends in Computer Graphics and Vision*, **2**, 259–362, 2006.

[43] S. C. Zhu, Y. N. Wu, D. B. Mumford. Minimax entropy principle and its application to texture modeling. *Neural Computation*, **9**, 1627-1660, 1998.